Final Draft
of the original manuscript:

Vautard, R.; Moran, M.D.; Solazzo, E.; Gilliam, R.C.; Matthias, V.;
Bianconi, R.; Chemel, C.; Ferreira, J.; Geyer, B.; Hansen, A.B.;
Jericevic, A.; Prank, M.; Segers, A.; Silver, J.D.; Werhahn, J.; Wolke, R.;
Rao, S.T.; Galmarini, S.:

Evaluation of the meteorological forcing used for the Air Quality Model Evaluation International Initiative (AQMEII) air quality simulations

In: Atmospheric Environment (2011) Elsevier

DOI: 10.1016/j.atmosenv.2011.10.065

Evaluation of the meteorological forcing used for the Air Quality Model Evaluation International Initiative (AQMEII) air quality simulations

Robert Vautard (1), Michael D. Moran (2), Efisio Solazzo (3), Robert C. Gilliam (4), Volker Matthias (5), Roberto Bianconi (6), Charles Chemel (7), Joana Ferreira (8), Beate Geyer (9), Ayoe B. Hansen (10), Amela Jericevic (11), Marje Prank (12), Arjo Segers (13), Jeremy D. Silver (10), Johannes Werhahn (14), Ralf Wolke (15), S.T. Rao (4), and Stefano Galmarini (3)

(1) Laboratoire des Sciences du Climat et de l'Environnement, IPSL Laboratoire CEA/CNRS/UVSQ, Orme des Merisiers, F-91191 Gif/Yvette CEDEX, France
(2) Air Quality Research Division, Science and Technology Branch, Environment Canada, 4905 Dufferin Street, Toronto, Ontario, M3H 5T4, Canada
(3) European Commission, Joint Research Centre, Institute for Environment and Sustainability, Ispra, Italy
(4) Atmospheric Modeling and Analysis Division, National Exposure Research Laboratory, Office of Research and Development, U.S. Environmental Protection Agency Research, Triangle Park, NC 27711 USA
(5) Institute of Coastal Research, Helmholtz-Zentrum Geesthacht, Germany
(6) Enviroware srl, via Dante 142, I-20863 Concorezzo (MB), Italy
(7) National Centre for Atmospheric Science (NCAS), Centre for Atmospheric & Instrumentation Research (CAIR), University of Hertfordshire, College Lane, Hatfield, Herts AL10 9AB, UK
(8) CESAM & Department of Environment and Planning, University of Aveiro, 3810-193 Aveiro, Portugal
(9) Institute of Coastal Research Helmholtz-Zentrum Geesthacht
(10) Department of Atmospheric Environment, National Environmental Research Institute, Aarhus University, Denmark
(11) Meteorological and Hydrological Service in Croatia, Zagreb, Croatia
(12) Finnish Meteorological Institute, Helsinki, Finland
(13) Netherlands Organisation for applied scientific research (TNO), Earth Environmental and Life Sciences, Princetonlaan 6, NL-3584CB Utrecht, The Netherlands
(14) Institute for Meteorology and Climate Research Atmospheric Environmental Research, Garmisch Partenkirchen
(15) Leibniz Institute for Tropospheric Research, Permoserstr. 15, 04318 Leipzig, Germany

10 May 2011, Submitted to *Atmospheric Environment (Special issue AQMEII)*

Abstract

Accurate regional air pollution simulation relies strongly on the accuracy of the mesoscale meteorological simulation used to drive the air quality model. The framework of the Air Quality Model Evaluation International Initiative (AQMEII), which involved a large international community of modeling groups in Europe and North America, offered a unique opportunity to evaluate the skill of mesoscale meteorological models for two continents for the same period. More than 20 groups worldwide participated in AQMEII, using several meteorological and chemical transport models with different configurations. The evaluation has been performed over a full year (2006) for both continents. The focus for this particular evaluation was meteorological parameters relevant to air quality processes such as transport and mixing, chemistry, and surface fluxes. The unprecedented scale of the exercise (one year, two continents) allowed us to examine the general characteristics of meteorological models' skill and uncertainty. In particular, we found that there was a large variability between models or even model versions in predicting key parameters such as surface shortwave radiation. We also found several systematic model biases such as wind speed overestimations, particularly during stable conditions. We conclude that major challenges still remain in the simulation of meteorology, such as nighttime meteorology and cloud/radiation processes, for air quality simulation.

1. Introduction

Air quality (AQ) modeling has progressed significantly over the past decade. It has evolved from the investigation of limited case studies of a few days or weeks duration to operational use for decision makers. Models are now routinely used to produce operational AQ forecasts in several countries (Brandt et al., 2001; McHenry et al., 2004; McKeen et al., 2005; Otte et al., 2005; Tarasick et al., 2007; Honoré et al., 2008; Hogrefe et al., 2007) and to provide a prospective evaluation of air pollutant emissions control scenarios for policy needs, as in the Clean Air For Europe program or the United States (U.S.) NOx State Implementation Plan Call (e.g., Amann et al., 2005; Gilliland et al., 2008; Gego et al., 2007). However, many uncertainties still remain and need to be reduced in order to improve the performance of such modeling systems so they would have high societal utility. Owing to the large number of interrelated processes in AQ models, biases in the representation of different processes are sometimes difficult to parse because of compensating errors, making it difficult to fully diagnose and attribute the different sources contributing to modeling uncertainty.

Uncertainties in AQ model simulations basically arise from three main classes of processes: (1) chemistry and aerosol physics; (2) fluxes (emissions, deposition, boundary fluxes); and (3) meteorological processes affecting transport and diffusion, chemistry, and surface fluxes (e.g., Pielke and Uliasz, 1998; Seaman, 2000). This paper looks at the influence of the last class of processes. More precisely, it will focus on the meteorological processes and parameters known to have a strong influence on air pollutant concentrations and their variability.

The three-dimensional wind fields transport primary pollutants or, if chemical reactions occur en route, secondary pollutants from emissions sources to receptor areas. Wind speed overestimation typically result in the underestimation of primary pollutant concentrations through increased ventilation and dilution, but they can also increase the concentrations of secondary pollutants near certain sources. For example, in areas close to nitric oxide (NO) emissions sources, an overestimated wind speed may induce a change in the photochemical regime since over-dilution of NO concentration will reduce ozone titration by NO, thereby resulting in an overestimation of ozone in the near-field. Wind direction errors will affect the path of pollutant trajectories and, hence, the source-receptor relationships. The concentration of pollutants in the lower troposphere, especially at the ground level, is also strongly sensitive to the rate of pollutant mixing by atmospheric turbulence, the height of the planetary boundary layer (PBL), and the amount of venting to the free troposphere. Atmospheric turbulence is, in turn, controlled by the magnitude of vertical temperature gradient and wind shear.

Meteorological parameters driving chemical processing are numerous. Radiation and its variability due to the presence of clouds, water vapor, and temperature are strong chemistry and aerosol thermodynamics drivers. For example, excessive cloud formation predicted at any altitude leads to the underestimation of below-cloud secondary pollutant formation from gas-phase processes and an overestimate in aerosol scavenging, inducing a low bias in secondary organic aerosol concentration. Many chemical reaction rates are temperature-dependent. And aerosol activation and aqueous-phase chemistry can occur in fog and clouds. Finally, meteorological processes also drive surface fluxes (emissions, deposition). Temperature and shortwave radiation control the emission of biogenic volatile organic compounds by vegetation, and wind speed and soil moisture control wind-blown dust emissions. Dry deposition is influenced by radiation, wind speed/turbulence, temperature, and surface wetness, and wet deposition is influenced by precipitation intensity and form (e.g., drizzle, rain, snow) (Gilliam et al., 2011).

Seaman (2000) provided an extensive overview of the influence of meteorology in regional AQ modeling in which he gave a number of examples of the sensitivity of AQ predictions to different meteorological variables. Hanna et al. (2001) employed a Monte Carlo approach to investigate the impact of uncertainties of 128 input variables, including a number of meteorological parameters, on ozone predictions made by a regional photochemical grid model (UAM-V). They found that the

UAM-V predictions were sensitive to wind speed and direction, relative humidity, and cloud cover. Zhang et al. (2007) followed a meteorological ensemble approach in which they considered small initial perturbations in wind and temperature on MM5 meteorological forecasts and their subsequent impact on ozone levels in Houston, Texas predicted by the Community Multiscale Air Quality (CMAQ) model (Byun and Schere, 2006) for an episode in summer 2000. For this particular episode, they found high uncertainties in predicted ozone.

A number of studies have considered the impact of supplying meteorological fields for the same case from two or more different mesoscale meteorological models to the same regional AQ model (Sistla et al., 1996; Biswas and Rao, 2001; Hogrefe et al., 2001; Smyth et al., 2006; Pirovano et al., 2007; de Meij et al., 2009; Appel et al., 2010). Biswas and Rao (2001) used two different prognostic meteorological models (MM5 and RAMS) with the UAM-V AQ model and found an uncertainty of about 20% in simulating episodic 1-h ozone maxima. Hogrefe et al. (2001) evaluated temperature, water vapor mixing ratio, and wind speed predictions from two different prognostic meteorological models (MM5 and RAMS3b) and found that model predictions were best for temperature and worst for wind speed and that neither model showed skill in predicting intra-day variability (i.e., periods less than 12 hours). Smyth et al. (2006) examined predictions of temperature, relative humidity, and wind speed from two different prognostic meteorological models (GEM and MM5) and found that differences in these fields resulted in a range of differences in O_3, PM_{10}, $PM_{2.5}$, and speciated $PM_{2.5}$ fields predicted by the CMAQ AQ model. de Meij et al. (2009) used two different prognostic meteorological models (MM5 and WRF) with the CHIMERE AQ model for winter and summer simulations of air quality in the Po Valley of Italy and found differences of 60% in PM_{10} predictions, particularly in the wintertime when predictions of PBL height made by the two meteorological models were significantly different. Finally, Appel et al. (2010) compared predictions made by CMAQ driven by two prognostic meteorological models (MM5 and WRF) and attributed differences in predicted AQ fields to differences in predicted wind speed, PBL height, cloud cover, and friction velocity.

Weather Services and research groups of more than 20 European countries investigated the influence of mesoscale meteorological models on regional AQ simulations in the framework of COST 728 (www.cost728.org). Eleven different AQ modeling systems participated in an inter-comparison exercise. The task was to model concentrations of particulate matter (PM) during a complex high-pressure episode over Germany in winter 2003 (Stern et al., 2008). It was found that none of the chemical transport models (CTMs) was able to predict the observed high PM values in East Germany (Matthias et al., 2010). The largest meteorological influence on the simulated concentrations was connected with vertical mixing of the pollutants. However, it could not be concluded that the most accurate model results for meteorological quantities led to the most accurate CTM results since emission inventories that drive AQ models are uncertain. In some cases errors in the meteorological and AQ models cancelled out, resulting in reasonable pollutant concentration values. One of the conclusions of the COST action was that extensive meteorological model testing on longer time scales is necessary to gain more insight into the meteorological effects that may cause errors in AQ modeling.

The framework of the Air Quality Model Evaluation International Initiative (AQMEII; Rao et al., 2011) offers a unique opportunity to evaluate AQ model strengths and weaknesses from a year-long AQ simulation for 2006 carried out by a large set of AQ models over two continents. This paper focuses on uncertainties associated with the meteorological inputs used by the AQMEII AQ modelers. It benefits immensely from the opportunity to inter-compare the performance of more than 10 meteorological models or model configurations for the same meteorological parameters on the same analysis grids for the same extended period for two continental-scale regions.

The AQMEII project has collected both meteorological observations of several meteorological parameters and asked participating modeling groups to extract equivalent model values in a format that it would allow direct comparison. However, the limited number of parameters routinely observed does not allow a full and comprehensive evaluation. Thus, we focus our analysis on a few issues. The main questions we address here concerning transport and mixing are:

- Are boundary-layer wind speed, PBL height, and its thermal structure, accurately simulated?
- Are boundary-layer temperature, relative humidity profiles, and surface radiation influencing atmospheric chemistry accurately simulated?
- Are meteorological processes influencing surface fluxes (surface temperature, wind speed, shortwave radiation, and precipitation) accurately simulated?
- What are the spatial and seasonal distribution of the biases in both mean and variability of the studied parameters?
- Are there any systematic differences in the prevailing meteorology over the two continents?

It must be noted that the questions addressed here relate strictly to the ability of models to *simulate* in retrospect and not *forecast* the meteorology of the lower troposphere. Because data assimilation is used, it is assumed that atmospheric model simulations are “best attempts” to reconstruct the state of the atmosphere retrospectively at a scale relevant to simulated air quality. This is generally done in two steps: an analysis or a reanalysis is carried out by a weather centre by blending cycling forecasts with new observations, followed by a simulation using a limited-area model with increased resolution and detailed surface and boundary-layer processes that may be combined with some form of data assimilation like analysis nudging. Our conclusions thus do not necessarily apply to weather forecasts, for which the additional uncertainty due to the forecast itself must be taken into account. However, they do help to quantify current uncertainties in a number of important meteorological parameters required by AQ simulation models. Finally, it should be noted that this study only provides investigation and evaluation of multi-model performance in general terms, and specific in-depth performance evaluations are also being carried out of individual models (e.g. Gilliam et al., 2011).

In addition to the evaluation and inter-comparison of the predictions of 2006 meteorology for North America (NA) and Europe (EU) made by the different meteorological models applied in the AQMEII study, this paper also reviews the weather conditions experienced during 2006 over both continents and the climatological representativeness of that year. After a description of the meteorological observations for 2006 in Section 2 and the AQMEII 2006 meteorological simulations in Section 3, a summary of 2006 weather is given in Section 4. Section 5 contains a quantitative multi-parameter evaluation of the set of meteorological simulations, and the paper concludes with a discussion of results and conclusions in Section 6.

2. Meteorological Observations

Surface-based observations for the evaluation of the annual Weather Research and Forecasting (WRF) model NA simulations were extracted from the Meterological Assimilation Data Ingest System (MADIS: http://madis.noaa.gov/) database. MADIS has both archived and real-time meteorological observations for North America including standard US and Canadian managed surface measurements as well as mesonet, rawinsonde, wind profiler, aircraft, and satellite measurements. For the European domain, the surface observations were extracted from the National Center for Atmospheric Research (NCAR) global synoptic surface data archive (http://dss.ucar.edu/datasets/ds464.0). The extracted observations for 10-m wind (speed and direction), 2-m temperature, 2-m relative humidity and precipitation were ingested by the ENSEMBLE system of the European Commission Joint Research Centre at Ispra, Italy (Galmarini et al. 2001, Bianconi et al. 2001, Galmarini et al. 2004), which allows matching in time and space with the various model datasets in order to carry out model performance evaluations. Some technical difficulties prevented the extraction of precipitation and relative humidity for the European domain, so the evaluation of these parameters is only for the North American domain. Since a robust, high resolution gridded precipitation dataset called the Parameter-elevation Regressions on Independent Slopes Model (PRISM) was available, the only direct evaluation of model precipitation is focused on the United States. The 4 km PRISM precipitation was aggregated up to the 12 km WRF grid so a direct comparison of seasonal precipitation could be made.

For upper-air analysis, meteorological variables observed from ozone soundings were downloaded from the WMO World Ozone and Ultraviolet Radiation Centre (www.woudc.org). Even though we do not investigate ozone in this article, this choice was made in order to have collocation with ozone measurements. Vertical profiles of pressure, temperature, relative humidity and wind speed were obtained from these soundings. In this study, a set of six stations was selected for each continent to serve as basis for model error statistics at the given altitudes of 0, 100, 250, 500, 750, 1000, 1500, 2000, 3000, 4000, 5000, 6000, 7500 and 8500 m above ground level. These stations were selected in three ways:

- The data set should not be too small (i.e., it should contain 40 profiles or more)
- The station altitude should be close to the altitude of the respective model grid cell.
- The stations should cover different regions of the continent

3. Meteorological Models

AQMEII provided a 2006 meteorological reference simulation for each continent to all participants so as to encourage both maximum participation and model input harmonization, but the use of these simulations was not mandatory. The reference simulations for NA and EU were generated using the Weather Research and Forecasting (WRF) model version 3.1 (Skamarock et al., 2008) and MM5 (Dudhia, 1993), respectively. The choice of these two models was ad hoc as one group on each side of the Atlantic volunteered to share their meteorological simulations. For the study conducted in this paper, groups used five different meteorological models or model configurations to drive NA AQ simulations and 11 different meteorological models or model configurations to drive EU AQ simulations. In this article, we emphasize the two reference simulations, as more than one group made use of each of these simulations, but we also describe and evaluate the other meteorological simulations that were employed.

For NA, the Advanced Research WRF (ARW) core was employed, which is a fully-compressible, non-hydrostatic, mass-conserving numerical solver. The modeling domain has a horizontal grid scale of 12 km with 34 vertical levels extending from the surface to the 50 hPa pressure layer with 14 levels below 1 km and the first layer about 40 m thick. This 12-km domain aligns exactly with standard U.S. Environmental Protection Agency (EPA) modeling domains, including the 36-km modeling domain described in Otte (2008) and Gilliam et al. (2006) and the 12-km domain discussed in Gilliam and Pleim (2010) and Appel et al. (2010). The difference is that this AQMEII modeling domain was extended to the north and east in order to include some key emission sources in Canada. In addition to the domain used, most of the model physics and four-dimensional data assimilation (FDDA) techniques were adopted from previous U.S. EPA modeling research such as Otte (2008) and Gilliam and Pleim (2010), which provide guidance on using WRF and MM5 effectively for retrospective AQ modeling applications although Gilliam et al. (2011) does suggests an updated technique that reduces transport errors in the lower troposphere.

Among the WRF physics options used were the Rapid Radiation Transfer Model Global (RRTMG) long- and short-wave radiation (Lacono et al., 2008), Morrison microphysics (Morrison et al., 2009), and the Kain-Fritsch 2 cumulus parameterization (Kain, 2004). For the land-surface model (LSM) and planetary boundary layer (PBL) model, the Pleim-Xiu LSM (Xiu and Pleim 2001; Pleim and Xiu 2003) and Asymmetric Convective Model version 2 (ACM2) (Pleim 2007a; Pleim 2007b) were used. These physics schemes, in particular, were developed explicitly for retrospective AQ modeling as the LSM employs an indirect soil moisture and temperature nudging scheme (Pleim and Gilliam, 2009). The soil nudging limits the error growth of critical near-surface fields such as temperature and moisture by adjusting surface energy fluxes to minimize the difference between the simulated 2-m temperature and moisture and that provided by an analysis. The ACM2 PBL scheme is also used in the CMAQ AQ model, so its use in WRF allows the mixing of pollutants to be consistent with the mixing of heat, moisture, and momentum within the PBL or other mixed layers in the atmosphere. Initialization and nudging follow the strategy described in Gilliam and Pleim (2010).

For EU, MM5 was run with lateral and surface (sea-surface temperature) boundary conditions obtained from the European Centre for Medium Range Weather Forecast (ECMWF) operational analyses, with a 6-hour sampling rate. Initial conditions (soil and atmospheric variables) were also taken from ECMWF analyses. The configuration used is Version 3.7, with most parameterizations as described in Chiriaco et al. (2006). Nudging to ECMWF analyses is applied with a relaxation time of about 3 hours for temperature and wind, and 15 hours for humidity. The 2006 simulation was split into twelve 1-month long simulations with new initializations 6 hours (spin-up time) before the first day of each month.

The vertical grid contains 32 sigma layers from surface to the top of the atmosphere, with 9 layers below the first kilometer. The top of the first layer was taken at s=0.996 (about 40 m above the surface, thus the middle of the first layer is 20 m). The horizontal grid is taken along a Mercator projection, with grid spacing decreasing from south to north. It extends outside the chemical model grid imposed by the AQMEII coordinates (15°W – 35°E; 35°N – 70°N). The exact domain boundaries for MM5 are 18°W – 38°W and 33.3°N – 71.5°N. At 50°N, the grid size is about 20 km while it is about 10 km at the northern boundary and 25 km at the southern boundary.

The planetary boundary layer (PBL) is described using the MRF PBL scheme (Hong and Pan, 1996). The microphysics scheme is the Reisner2 scheme, which considers five states of water: vapor, rain, cloud, ice, and graupel (Reisner et al., 1998). The cumulus scheme is taken from Grell and Devenyi (2002). The NOAH LSM scheme is used (Ek et al., 2003), with the default four layer depths changed to 7, 28, 100, and 289 cm to better match ECMWF model soil levels. The long-wave radiation scheme used is the Rapid Radiation Transfer Model (RRTM; Mlawer et al., 1997).

In addition to these two meteorological reference simulations offered to AQMEII participants, some of the groups performed their own meteorological simulations. A total of six different meteorological models were used: COSMO, ECMWF, GEM, MM5, PARLAM-PS, and WRF. A summary of some of the main characteristics of all of the models is given in Table 1. There is considerable overlap between the models in terms of physical parameterizations and run strategies employed, but five NA and 11 EU meteorological model configurations were distinct. The horizontal grid spacing used ranged from 12 to 50 km, and the number of vertical levels ranged from 23 to 58. Data assimilation techniques were employed by a minority of the models.

In Section 5, the five NA meteorological model configurations are denoted by the labels “M1NA” to “M5NA” and the 11 EU configurations by the labels “M1EU” to “M11EU”. Three model configurations were applied for both 2006 NA and EU simulations and have been assigned the labels “M1NA” and “M1EU”, “M2NA” and “M2EU”, and “M3NA” and “M3EU”. Note that the order in which the labels have been assigned is different from the order of the model configuration descriptions in Table 1 to keep anonymity.

4. 2006 Weather in North America and Europe

For a number of years the U.S. National Climatic Data Center (NCDC) has led an effort to characterize the weather of recent years. Arguez et al. (2007) provides the summary of significant global weather events and anomalies in 2006. The highlights specifically for North America and Europe are covered here and will be used to provide context for the model evaluation where appropriate. One of the most significant characteristics of 2006 was its rank as the 5th warmest (global) in the last century.

Regionally, parts of Europe (UK, Spain and the Netherlands) saw the warmest year on record and parts of the U.S. and Canada experienced the second warmest year on record. Figure 1 provides the 850 hPa seasonal temperature anomaly, which clearly shows the warmer than normal weather. 500 hPa geopotential height anomalies (Figure 2) correlated well with the 850 hPa temperature anomalies as the regions with warmer than normal temperatures almost always correlate to more ridging aloft. The averaged temperature in January over U.S. was 3.9 K above normal, which is a full 1 K greater than the previous 100+ year record. Most of the central and western US was warmer than normal in the summer as well. Areas in the central and southwestern U.S. that saw the higher temperatures (Figure 1) and anomalous ridging aloft (Figure 2) also experienced very little rainfall and, as a result, severe drought conditions. A record-breaking heat wave that reinforced the drought conditions began in the northern Plains and upper Midwest in mid-July and spread to the western U.S. in late July then back to the east, all the way to the East Coast for the first half of August (Arguez et al., 2007).

The eastern U.S. and southern Ontario and Quebec experienced average to above average rainfall in the spring and summer. The 500 hPa height anomalies in Figure 2 indicate the east coast of North America did experience near to below normal 500 hPa height and temperature at 850 hPa (Figure 1) in the spring and summer, which translates to above average rainfall. On the opposite side of the Continent, areas of the Pacific Northwest U.S. and British Columbia saw heavy rainfall the last few months of 2006 because of blocking ridge in the NW Pacific (Arguez et al., 2007).

For Europe, Arguez et al. (2007) showed annual near-surface temperature anomalies that were generally greater than 0.5-1.0 K for most of Europe. An examination of the seasonal 850 hPa temperature and 500 hPa geopotential height anomalies in Figure 1 and Figure 2, respectively, shows cooler than normal temperature and lower 500 hPa heights for the first part of 2006 across much of Europe. Arguez et al. (2007) identifies this large-scale weather pattern as common feature with the negative phase of the North Atlantic Oscillation (NAO) that was in place for the first few months of

2006. Countries in the north and far western parts of Europe, like the British Isles and Scandinavia, saw temperatures at or slightly above normal and normal precipitation in the winter of 2006.

The large-scale weather pattern made a transition from cooler and drier over much of Europe in winter to warmer than normal, in general, for the rest of 2006. However, there was a substantial month-to-month variability from spring to summer that the seasonal anomalies do not capture well. For example, July 2006 was well above normal as an eastward extension of the Azores High developed over central Europe leading to an extreme heat wave (Arguez et al., 2007). Many of the central European countries, including Belgium, Netherlands, Germany, Czech Republic and Austria, set all-time records in terms of mean July temperatures. This heat wave was also accompanied by a large-scale pollution episode over Central Europe (Struzewska and Kaminski, 2008). In August however, this warm pattern transitioned to a cooler than normal pattern. Precipitation was generally lower than normal during the anomalously high temperatures and near or just above normal during the cooler periods like what occurred in August.

Autumn was the most anomalous season of the year over Europe. It broke the record of seasonal temperature by a large amount and was shown to have a temperature largely exceeding that expected from analogue weather regimes in previous years (Yiou et al., 2007), presumably due to a concurrence of a large Atlantic sea surface temperature anomaly and a persistent southerly flow (Cattiaux et al., 2009). The 850 hPa temperature anomaly for autumn clearly shows that a large anomaly that had been centered in the Northern Hemisphere (+3.0 K) was now centered over the Denmark/Germany area and extended north to Scandinavia, west to the British Isles and south to France as well as much of southern Europe that borders the Mediterranean Sea. The 500 hPa height anomalies are in good agreement with the warm autumn temperatures as a persistent ridging is centered over Germany and Poland. Precipitation amounts under and around this ridge, as one would expect, were well below normal. Areas that did experience higher than normal autumn precipitation are those countries to the west and southwest periphery of the 500 hPa ridge anomaly, which includes Ireland, United Kingdom, western France and western Spain and Portugal. Much of Europe that borders the Mediterranean was dry as the axis of the 500 hPa ridge anomaly extended south into the Mediterranean Sea between Spain and Italy as shown by Figure 2 and describe in detail by Arguez et al. (2007).

5. Quantitative Evaluation

In this section, we quantitatively compare model simulations and observations of weather parameters that are most relevant to air quality. For the sake of synthesis, we have focused on three distinctive subregions on each continent that have qualitatively different climate and air quality characteristics. These subregions are shown in Figure 3, together with the locations of meteorological measurement sites.

For NA, subregion NA1, the southwestern U.S., was selected because of the combination of high solar radiation, low relative humidity, large cities with poor air quality (Los Angeles, Phoenix), and geographic location to the west of the Rocky Mountain barrier. Subregion NA2, the Texas area, was selected for its hot, humid climate, large cities with poor air quality (Houston, Dallas), and location to the east of the Rocky Mountain barrier. Subregion NA3, northeastern NA including parts of Canada, has a marked seasonal cycle, three of the North American Great Lakes, the highest emissions areas in NA, and large cities (New York City, Philadelphia, Toronto, Montreal). For EU, subregion EU1, the British Isles and western France, was selected for its mid-latitude, mixed maritime-continental climate and large cities (London, Paris). Subregion EU2, Central Europe, has a rather continental climate with marked seasonality, many large cities, and large emissions areas. Subregion EU3, the Po Valley of Italy, has a Mediterranean climate, poor air quality, and belongs to a separate air shed from northern Europe due to the Alpine barrier.

5.1 Transport and mixing

The weather parameters that drive the transport and mixing of air pollutants are controlled by grid-scale winds and subgrid-scale turbulence. We use here the reduced set of available routine network observations described in Section 2. For resolving transport, the analysis uses the 10-m wind observations and vertical wind profiles obtained from ozonesonde launches.

Figure 4 shows the evolution of the 10-m wind speed averaged over all measurement station locations in each subregion for each calendar month for each model and for the observations. In general the seasonal cycle is well reproduced by all models in all subregions, but wind speed amplitude spread is rather large and overestimated for EU. Model values differ by rather constant multiplicative factors. This could be due to a combination of differences in the model resolution in the lowest layers and differences in the methodology of diagnosing the 10 m wind amongst models. A general overestimation is found in all regions but NA1 and NA2, and no obvious explanation was found for this feature.

The amplitudes of the diurnal cycle of wind speed are underestimated (Figure 5). In the stable nighttime boundary layer, wind speed is overestimated, probably as a result of the lack of vertical resolution (i.e., layer height is approximately 40m) and overly strong vertical diffusion. For the NA subregions, the intensification of wind speed due to the stronger vertical momentum fluxes that are associated with the development of the convective boundary layer and associated increase in wind speed is not marked enough and daytime wind speeds are generally underestimated. However, biases are generally larger during the night, which indicates a general difficulty to simulate the stable boundary layer. A particular situation occurs for EU3 (the Po Valley) where even the shape of the diurnal cycle is not well simulated, probably due to the complex topography of the area and the land-sea interface that induces complex mesoscale circulations.

The skill of the models in simulating the day-to-day variability of daily mean wind speed is summarized in Figure 6, which shows Taylor diagrams (Taylor, 2001) for wind speeds in all subregions studied. In all subregions, simulations have a correlation exceeding 0.5, and often reaching 0.9. For

NA, the amplitude of daily wind variability varies by a factor of two relative to the observed one, with no systematic bias, while the variability is overestimated by all models in the EU case, which is consistent with the general overestimation of wind speed. Over NA, there is a marked spread in model skill. Correlation is generally higher for NA2 and NA3, where three models have a correlation exceeding 0.9, than for NA1, where topographic and coastal effects dominate the meteorology. For EU, models' skill is higher in maritime areas (EU1) and Central Europe (EU2), but is poor over the Po Valley due to complex topography. The large spread in model skill leads to a skill of the ensemble mean or median that is not higher than that of any model.

The spatial distribution of surface wind speed is fairly well simulated by the models (Figure 7). Over NA, the differences between the windier mid-western areas and less windy eastern areas are correctly reproduced, even though the observed winds are somewhat weaker than the simulated winds. WRF also generally does well in simulating the strength of transport over the oceans. Over EU, MM5 reproduces the northwest – southeast wind speed gradient. Regional discrepancies are found, for example, in some mountainous areas (e.g., Scandinavia and Alpine regions), where poorly resolved effects of topography probably explain the simulated wind overestimation.

Vertical profiles (based on ozone soundings) of wind speed are compared to the results of several models over NA and EU (Fig. 8). The statistical measures (bias, RMSE, correlation), were calculated for each of the stations and then averaged. Wind speed is well simulated along the profiles but markedly overestimated at lower altitudes for EU, confirming the results for 10-m wind speed. For NA, more scatter occurs among models for wind, but agreement between model and observations in terms of the mean wind speed is stronger in the lowest 500 m for three of the models. The RMSE is between 2 and 4 m s^{-1} (except for models M1NA and M2NA in North America) with slightly higher values in higher altitudes, which corresponds to higher wind speeds on average. The correlation is lowest close to ground, but may exhibit values exceeding 0.9 above 500 m in Europe and above 1500 m in North America. Two models (M1NA, M2NA) show poor correlation of 0 – 0.25 in North America.

For simulating North America, the results from the European groups show clearly less agreement with the observations compared to Canadian and U.S. groups. However it must be taken into account that different run schemes and nudging techniques are used (see Table 1). If a model run is restarted every few days with initial conditions that stem from reanalysis data, the results will stay close to the observations because they are typically considered in the reanalysis. A continuous model run on the other hand, that is only nudged to the wind fields above the PBL has much more freedom to develop differently than the driving reanalysis fields. This should lead to a larger variability of the simulated quantities and therefore larger RMSE and lower correlation.

In order to evaluate the skill of the model in representing turbulent mixing, PBL heights calculated by the different meteorological models are compared to observations at Lindenberg, Germany (14.3°E, 52.1°N). The observational data has been derived from radiosondes using the bulk Richardson number method. The observational data has been derived from radiosondes using profiles of the bulk Richardson number Ri_b. The method is a standard and widely used approach to derive PBL height from the numerical weather prediction (NWP) models, as well as from the radiosounding data (see e.g. the review by Seibert et al., 2000). Here, a critical Richardson number $Ri_c = 0.2$ was chosen. The top of the PBL is the altitude where $Ri_b > Ri_c$.

Each model has its own algorithm to diagnose the PBL height, many of them are based on similar approaches as the one applied to the observations. It was found that the models are able to simulate the PBL height at noon quite well (Fig. 9 and Table 2). This can be interpreted in a way that the PBL parameterizations are working reasonably well and the vertical mixing of pollutants under these conditions is likely represented adequately in the models. By contrast, particularly at 18 UTC and in the summer months, the modeled PBL height is much lower than observed (Fig. 9). This may be explained by the fact that this is a transition time to a stable PBL as static stability of the surface layer turns positive. In this transition phase the top of the PBL is not well defined and the models typically diagnose the top of the PBL to be one of the first few model layers while the radiosondes do not show this. Some of the models give very low PBL height around the top of the first model layer throughout the night which is clearly unrealistic, but default position of these non-TKE schemes. The morning ascent of the PBL, when strong mixing processes take place, could not, unfortunately, be investigated due to 6-hour observation sampling.

Table 2 gives the mean observed PBL heights at 0, 6, 12 and 18 UTC together with the bias, RMSE and the correlation of the model results when compared to the observations. Here, all observations including those when the PBL height was not well defined were taken into account. As mentioned above, the largest discrepancies between model results and observations occur at 18 UTC, at this time none of the models reproduce the observed values with reasonable accuracy. This is represented in poor correlation coefficients and a large negative bias. About 3-5 models show clear problems in representing the correct PBL height at all times except 12 UTC.

5.2 Chemistry drivers

Three of the meteorological parameters that drive atmospheric processing of emissions (chemistry and aerosol transformations, see Monks et al., 2009 for a full review) are evaluated here: temperature, relative humidity and surface shortwave radiation. Biases of monthly means of 2-m temperature are generally small (Figure 10). Over NA only one model has a moderate positive temperature bias that occurs mainly in the winter season and is as large as 5 K. Otherwise, the remaining ensemble members have little spread and agree well with the observed temperature in a regional average sense. Likewise, in EU, biases remain small, with slightly more spread during winter months, but the model ensemble envelopes the observations well.

The diurnal cycles of 2-m temperature are also fairly well reproduced by the models (Figure 11). Unlike the 10-m wind speed, the amplitudes of the diurnal cycles for 2-m temperature are not underestimated except for one model over NA, which also had the systematic positive wind speed bias seen in Figure 5. Thus we expect that related temperature-dependent fields (clouds, longwave radiation and sensible heat fluxes, see e.g. Liu et al., 2003) are fairly well accounted for in the models.

The typical vertical temperature profile bias is between ±1 K (Figure 12). On average the temperature is slightly underestimated by the models. The RMSE is between 1 and 2 K along the profile, best agreement being achieved between 1000 and 6000 m altitude. The correlation is above 0.9, and at many heights, even above 0.95.

For simulated ozone episodes to build up, it is essential that the highest diurnal temperatures are well predicted by the models, other parameters also being important. In order to focus on this issue, Figure 13 shows the 99.5th centiles of the models temperature distribution (hourly values) against the corresponding observed 99.5th centiles. In most cases, considering both continents, the extreme temperatures that were observed are greater than the model simulated temperatures. The differences, however, remain moderate and do not exceed 3 K. This small bias should have the effect of reducing gas-phase chemical reaction rates as well as slightly displacing the gas-particle equilibrium for volatile species.

Relative humidity (RH) influences photochemistry through reactions between water vapor and the oxygen radical, which forms the hydroxyl radical. Water vapor can be either an ozone sink or source, depending on the availability of nitrogen oxides. Relative humidity at 2 m is not as well simulated as temperature (Figure 14 vs. 10). Over NA, systematic biases are found for most models, and in general RH is overestimated. The bias is particularly marked over the southwestern U.S. (subregion NA1), the driest of the three NA subregions. This reveals model deficiencies in dry areas, with a possible consequence of overestimation of soil moisture. However, the amplitude of the diurnal cycle is simulated in a realistic manner (not shown).

Above the surface, relative humidity is overestimated by all models and in all regions (Figure 15), in agreement with surface analysis for NA. Biases and RMSE both increase with height. This is not surprising if one keeps in mind that the water vapor mixing ratio decreases rapidly with height and therefore RH is sensible to small deviations of the mixing ratio. The overestimation of RH might be connected with the underestimation of the temperature. The correlation of the time series, however, is relatively large, with values between 0.6 and 0.8.

Model predictions of hourly gridded surface shortwave radiation (SSWR) were submitted to AQMEII by most groups, but surface radiation components are not routinely measured at many stations in either NA or EU. Since shortwave radiation plays an important role in photochemistry, the surface energy budget, and biogenic emissions, it was still of interest to examine differences between models, especially because SSWR will be modulated by cloud shading, which may vary considerably between models due to the difficulties associated with predicting the presence and properties of clouds.

The lefthand column of Figure 16 shows the monthly variation of mean mid-day SSWR at the centers of the three NA subregions (see Fig. 3) predicted by four meteorological models. The highest summer values for the three subregions are predicted over the southwestern U.S. (NA1), and the largest differences between the models for this subregion occur in the spring (~400 Wm^{-2} or ~100%). The lowest summer values are predicted for northeastern NA (NA3), and the largest differences between models for this subregion occur in June (~400 Wm^{-2} or ~100%). These summertime differences are surprisingly large and are likely due to differences in the predictions of clouds. The righthand column of Figure 16 shows the same analysis for the center points of the three EU subregions for nine meteorological models or model configurations. The largest actual difference between models occurs in June for EU3 (~500 Wm^{-2} or ~125%) but relative differences are even higher in the winter months. For the EU subregions the ranking between models is generally constant between subregions and across seasons. These systematic differences in SSWR between models may impact many other meteorological fields such as surface temperature and PBL height.

Figure 17 shows considerable variation in the model-simulated diurnal cycle of SSWR for the six subregions. For NA there are systematic differences of 15% to 50% between the four models at local noon and for EU there are differences of 30% to 60% between eight models (excluding one outlier). As expected, the maximum daytime value tends to decrease with increasing latitude, but cloud cover also plays a role; for example, the maximum daytime value is lower for subregion NA2 (31°N) than for NA1 (36.5°N). For the EU subregions there is also a suggestion that local noon differs between two clusters of models.

Figure 18 shows monthly variations in the standard deviation of mid-day hourly SSWR for each month of 2006 for the same six locations. This quantity provides another measure of the impact of differences in model predictions of hourly cloud fields on cloud shading. It is evident that there are considerable differences between the models throughout the year, but these differences vary from subregion to subregion. The differences are largest in spring and summer for the southwestern U.S. (NA1) but fairly even throughout the year for northeast NA (NA3). For the Texas subregion (NA2) and the three EU subregions, on the other hand, there is closer agreement between the models in the cold season and less agreement in the warm season. One possible explanation is a higher frequency of stratiform cloud in the winter, a higher frequency of convective cloud in the summer, and closer agreement between model predictions of the former (see next section).

5.3 Surface fluxes

Biogenic emissions depend on a number of factors, including surface weather. Soil nitrogen oxides (NOx) and vegetation volatile organic compound (VOC) emissions increase nonlinearly with temperature, with sharp sensitivity at temperatures exceeding 30°C. The above analysis shows that these emissions should be fairly well represented in most models, but an underestimation may be expected due to moderate low temperature bias at highest temperatures. Biogenic VOC emissions also depend on radiation, but the model skill for radiation could not be properly evaluated against observations within this study.

A major driver of dry deposition fluxes is the stomatal resistance which also depends on temperature and radiation. Dry deposition, particularly for ozone, is also driven by turbulent mixing near the ground. Although we were not able to evaluate the model predictions of sensible heat fluxes, the weak differences between simulated and observed 2-m temperatures indicates that aerodynamic resistance should not undergo strong model biases.

For both aerosol particles and soluble gases, wet deposition fluxes depend on precipitation frequency, duration, intensity, and type (e.g., Wang et al., 2010). Model predictions of hourly precipitation for 2006 have been examined for the North American simulations. In terms of seasonal accumulation, Table 3 lists mean winter (Dec.-Feb.) and summer (June-Aug.) precipitation amounts for all measurement stations in each of the three NA analysis subregions and corresponding mean model-predicted precipitation amounts for these three groups of stations. In 2006, the NA1 subregion received more precipitation in the winter than the summer while the opposite was true for the NA2 and NA3 subregions. Most of the models reproduced this geographically-varying seasonal cycle, but there is a wide variation in predicted amount and the models, including the ensemble mean, tend to overpredict seasonal precipitation. This is particularly true in the summer when convective precipitation typically dominates (e.g., Tremblay, 2005), since the simulation of convective precipitation is challenging because of its small-scale and scattered nature.

Given that wintertime precipitation tends to be dominated by stratiform precipitation (Tremblay, 2005), and given that stratiform precipitation tends to be longer-lived with more wide spread coverage than convective precipitation due to its synoptic forcing, it is useful to examine observed and predicted hourly precipitation intensity. Figure 19 shows winter- and summer-season histograms of observed and predicted occurrence frequencies for different hourly precipitation amounts for the three NA analysis subregions. Both observations and models exhibit more high-intensity precipitation events (i.e., a longer distributional “tail”) in the summer than winter for subregion NA3, about the same for subregion NA2, and fewer high-intensity events in subregion

NA1. In meso-β-scale models (i.e., horizontal grid spacing of 10-40 km) such as those considered here, transport by convective precipitation systems will be associated with subgrid-scale circulations and hence will not be resolvable. Figure 19, however, suggests that such high-intensity precipitation occurs infrequently (note the semi-log scale). In terms of low-intensity precipitation forecasts, on the other hand, most of the models underpredict non-precipitation events (i.e., the "< 0.5" bin includes dry conditions and "trace" precipitation) but overpredict the occurrence of low-intensity precipitation (i.e., 1-5 mm h^{-1}). There is also considerable variability amongst the models. Note that it is likely that this difference between the measurements and models can be ascribed at least in part to the comparison here of point measurements to grid-scale predictions, which introduces the problem of representativeness error due to interpolation of model grid-cell values to station locations (e.g., Tustison et al., 2001). Nevertheless, the combination of higher accumulation, longer duration, and greater spatial coverage on average in the model predictions suggests that wet removal may be overemphasized by the models in areas of more frequent convection, leading to a tendency to underestimate ambient air concentrations of particles and water-soluble species such as SO_2, HNO_3, and NH_3.

Finally, Figure 20 compares the spatial distribution of seasonally observed precipitation (PRISM) for two seasons with the corresponding spatial distribution predicted by the U.S. EPA WRF simulation. WRF agrees with PRISM quite well in winter when grid-scale stratiform precipitation is likely dominant, whereas in summer, when diurnally-forced convective precipitation is most common, the PRISM and WRF differ significantly in total summer precipitation.

6. Summary

This study was devoted to a collective operational evaluation of regional meteorological models that forced the air quality simulations carried out in the AQMEII regional AQ modeling system intercomparison. It was the first time that a multi-model evaluation of this scale has been performed, with five participating meteorological models or model versions over North America (NA) and 11 models or model versions participating over Europe (EU). We emphasized model parameters that are major drivers of air quality variability. The focus was not to inter-compare the models and produce statistical metrics, but rather to discern general characteristics seen. This study produced a number of conclusions.

- There is considerable variability among model predictions, even for different configurations or post-processing of the same model. This is particularly clear for short wave radiation where noontime predicted values vary by a factor up to two. This scatter should contribute to variability in many other predicted fields, suggesting that prediction of the timing and location of clouds remains an ongoing challenge for both meteorological and AQ modeling.
- There are systematic positive model biases, particularly for EU, for surface and boundary-layer wind speed, which are confirmed both in 10-m wind and ozonesonde measurements. These biases contribute to a tendency to underestimate surface concentrations of primary pollutants. The overestimation is particularly marked in stable wintertime or nighttime conditions. The day-to-day variability of low-level wind speed is also systematically overestimated for EU.
- Developed planetary boundary layer (PBL) heights are, at one European site, well captured, but PBL height is poorly simulated at nighttime or transition times. Models generally underpredict PBL heights in these situations, which may lead to air pollutant concentration overestimation if this conclusion holds in other locations.
- Less clear conclusions hold for water vapor and precipitation, but we found large – albeit not systematic – differences for these parameters. These variables can significantly influence the predicted concentrations of fine particulate matter.
- The models have a tendency to underestimate the occurrence of non-precipitation conditions and extreme precipitation events but overpredict the occurrence of light to

moderate precipitation conditions. This could lead to an overestimation of wet removal of particles and water-soluble gases.

- Not surprisingly, temperature is the best predicted of the variables that we analyzed in this study.

Since the meteorological variables considered in this paper are known to have important influences on AQ predictions, the large variability in the predicted meteorological fields amongst the different meteorological models and model versions will likely make an important contribution to the variability in the predicted AQ fields that has been quantified in companion AQMEII papers in this special issue. For primary pollutants and aerosols, dispersion (wind, boundary layer height) is the most important concentration driver. From our analysis, we conclude that model simulations of daytime meteorology have fewer deficiencies than simulations of nighttime meteorology. Nighttime concentrations undergo systematic overestimation of wind and underestimation of PBL height, which is a potential source of large error compensation for pollutant simulation. Therefore, nighttime meteorology remains a challenge for models. Finally, for photochemistry and secondary pollutants, shortwave radiation and its influence on cloud processes is probably the most critical process to improve as it is a major driver of ozone build up. We conclude that efforts must be made to reduce the uncertainty in the simulation of radiation and clouds.

Acknowledgements

The authors would like to acknowledge the following data providers. NOAA and Environment Canada provided North American surface meteorological data from national monitoring networks. The Data Support Section of the National Center for Atmospheric Research (NCAR) in Boulder, Colorado provided European surface meteorological data. The WMO World Ozone and Ultraviolet Data Centre (WOUDC) and its data-contributing agencies provided vertical meteorological profiles from both the North American and European ozonesonde networks. PRISM Climate Group, Oregon State University (http://www.prismclimate.org**)** provided the gridded observed precipitation.

Boundary layer height data from radiosoundings at Lindenberg for 2006 have been kindly provided by Frank Beyrich from Meteorological Observatory Lindenberg - Richard-Aßmann-Observatory of the German Meteorological Service (DWD). The authors would also like to thank following individuals for their assistance: Junhua Zhang and Radenko Pavlovic of Environment Canada, Ana Isabel Miranda and Alexandra Monteiro of the University of Aveiro, Luksa Kraljevic from the meteorological service in Croatia, and Anna Carlin Benedictow. The present study is partially funded by the Center for Energy, Environment and Health, financed by The Danish Strategic Research Program on Sustainable Energy under contract no 2104-06-0027. French teams acknowledge the LEFE/CHAT program of the Institut National de Sciences de l'Univers (INSU) through the support of the national AQMEII.fr project grant.

References

Amann, M., Bertok, I., Cofala, J., Gyarfas, F.., Heyes, C., Klimont, Z., Schöpp, W., Winiwater, W., 2005. Clean Air for Europe (CAFE) program final report, Int. Inst. for Appl. Syst. Anal., Laxenburg, Austria.

Appel, K.W., Roselle, S.J., Gilliam, R.C., Pleim, J.E., 2010. Sensitivity of the Community Multiscale Air Quality (CMAQ) model v4.7 results for the eastern United States to MM5 and WRF meteorological drivers. Geoscientific Model Development 3, 169-188.

Arguez, A., Waple, A.M., Sanchez-Lugo, A.M., 2007. State of the climate in 2006: Executive summary. Bulletin of the American Meteorological Society 88, 929-932 + Supplement.

Belair, S., Crevier, L.-P., Mailhot, J., Bilodeau, B., Delage, Y., 2003. Operational implementation of the ISBA land surface scheme in the Canadian regional weather forecast model. Part I: Warm season results. Journal of Hydrometeorology 4, 352–370.

Betts, A. K., and M. J. Miller, 1993: The Betts-Miller scheme. The representation of cumulus convection in numerical models, K. A. Emanuel and D. J. Raymond, Eds., Amer. Meteor. Soc., 246 pp.

Bianconi R., S. Galmarini and R. Bellasio, A WWW-based decision support system for the management of accidental releases of radionuclides in the atmosphere. *Environmental Modelling & Software*, **19**, 401–411, 2004.

Biswas, J., Rao, S.T., 2001. Uncertainties in episodic ozone modeling stemming from uncertainties in the meteorological fields. Journal of Applied Meteorology 40, 117-136.

Brandt, J., Christensen, J.H., Frohn, L.M., Berkowicz, R., 2001. Operational air pollution forecasts from regional scale to urban street scale. Part 2: Performance evaluation. Physics and Chemistry of the Earth, Part B., 26, 825–830, doi:10.1016/S1464-1909(01)00092-2.

Byun, D., Schere, K.L., 2006. Review of the governing equations, computational algorithms, and other components of the Models-3 Community Multiscale Air Quality (CMAQ) modeling system. Applied Mechanics Reviews, 59, 51-77.

Cattiaux, J., Vautard, R., Yiou, P., 2009. Origins of the extremely warm European fall of 2006. Geophysical Research Letters 36, doi: 10.1029/2009GL037339, 5 pp.

Chen, F., and J. Dudhia, 2001: Coupling an advanced land-surface/hydrology model with the Penn State/NCAR MM5 modeling system. Part I: Model description and implementation. *Mon. Wea. Rev.,* 129, 569–585.

Chiriaco, M., Vautard, R., Chepfer, H., Haeffelin, M., Wanherdrick, Y., Morille, Y., Protat, A., Dudhia, J., 2006. The ability of MM5 to simulate ice clouds: systematic comparison between simulated and measured fluxes and lidar/radar profiles at SIRTA atmospheric observatory. Monthly Weather Review 134, 897-918.

Côté, J., Desmarais, J.-G., Gravel, S., Méthot, A., Patoine, A., Roch, M., Staniforth, A., 1998a. The operational CMC/MRB Global Environmental Multiscale (GEM) model. Part I: Design considerations and formulation. Monthly Weather Review 126, 1373-1395.

Côté, J., Desmarais, J.-G., Gravel, S., Méthot, A., Patoine, A., Roch, M., Staniforth, A., 1998b. The operational CMC/MRB Global Environmental Multiscale (GEM) model. Part II: Results. Monthly Weather Review 126, 1397-1418.

de Meij, A., Gzella, A., Cuvelier, C., Thunis, P., Bessagnet, B., Vinuesa, J.F., Menut, L., Kelder, H.M., 2009. The impact of MM5 and WRF meteorology over complex terrain on CHIMERE model calculations. Atmospheric Chemistry and Physics 9, 6611-6632.

Doms, G., Schättler, U., 2004. A description of the nonhydrostatic regional COSMO-Model. Part II: Physical parametrizations. Deutscher Wetterdienst, Offenbach [available from http://www.cosmo-model.org].

Doms, G., Forstner, J., Heise, E., Herzog, H.-J., Raschendorfer, M., Reinhardt, T., Ritter, B., Schrodin, R., Schulz, J.-P., Vogel, G., 2007. A description of the nonhydrostatic regional COSMO-Model. Part II:

Physical parametrizations. Deutscher Wetterdienst, Offenbach [available from http://www.cosmo-model.org].

Dudhia, J., 1993. A nonhydrostatic version of the Penn State–NCAR mesoscale model: Validation tests and simulation of an Atlantic cyclone and cold front. Monthly Weather Review 121, 1493–1513.

Dudhia, J., 1996: A multi-layer soil temperature model for MM5. Preprints, The Sixth PSU/NCAR Mesoscale Model Users' Workshop, 22-24 July 1996, Boulder, Colorado, 49-50. Available from http://www.mmm.ucar.edu/mm5/mm5v2/whatisnewinv2.html.

Ek, M.B., Mitchell, K.E., Lin, Y., Rogers, E., Grunmann, P., Koren, V., Gayno, G., Tarpley, J.D., 2003. Implementation of Noah land surface model advances in the National Centers for Environmental Prediction operational mesoscale Eta model. Journal of Geophysical Research 108, D22/8851.

Galmarini S., Bianconi R., Bellasio R., Graziani G., Forecasting consequences of accidental releases from ensemble dispersion modelling, 2001, *Journal of Environmental Radioactivity* 57, 203-219.

Galmarini S., , R. Bianconi, W. Klug, T. Mikkelsen, R. Addis, S. Andronopoulos, P. Astrup, A. Baklanov, J. Bartnicki, J. C. Bartzis, R. Bellasio, F. Bompay, R. Buckley, M. Bouzom, H. Champion, R. D'Amours, E. Davakis, H. Eleveld, G. T. Geertsema, H. Glaab, M. Kollax, M. Ilvonen, A. Manning, U. Pechinger, C. Persson, E. Polreich, S. Potempski, M. Prodanova, J. Saltbones, H. Slaper, M. A. Sofiev, D. Syrakov, J. H. Sørensen, L. Van der Auwera, I. Valkama, R. Zelazny, 2004: Can the Confidence in Long Range Atmospheric Transport Models be increased? The Pan European experince of ENSEMBLE*, Radiation Protection Dosimetry* 109, 1-2, 19-24.

Gego, E., P.S Porter, A. Gilliland, S.T. Rao. Observation-based assessment of the impact of nitrogen oxides emissions reductions on O3 air quality over the eastern United States. Journal of Applied Meteorology and Climatology, 46, 994-1008, 2007.

Gilliam, R.C., Hogrefe, C., Rao, S.T., 2006. New methods for evaluating meteorological models used in air quality applications. Atmospheric Environment 40, 5073-5086.

Gilliam, R.C., Pleim, J.E., 2010. Performance assessment of new land-surface and planetary boundary layer physics in the WRF-ARW. Journal of Applied Meteorology and Climatology 49, 760-774.

Gilliam, R. C., J.M. Godowitch, W. Appel, and ST Rao, 2011: Improving the Characterization of Lower Troposphere Transport with Four Dimensional Data Assimilation. J. Geophys. Res., submitted.

Gilliland, A.B., Hogrefe, C., Pinder, R.W., Godowitch, J.M., Foley, K.L., Rao, S.T., 2008. Dynamic evaluation of regional air quality models: Assessing changes in O_3 stemming from changes in emissions and meteorology. Atmospheric Environment 42, 5110-5123.

Grasselt, R., Schüttemeyer, D., Warrach-Sagi, K., Ament, F., Simmer, C., 2008. Validation of TERRA-ML with discharge measurements. Meteorologische Zeitschrift, Vol. **17**, No. 6, 763-773.

Grell, G., Dudhia, J., Stauffer, D. (1994). A Description of Fifth-Generation Penn State/NCAR Mesoscale Model (MM5), NCAR Tech. Note NCAR/TN-398+STR, Boulder, pp. 122.

Grell, G.A., Devenyi, D., 2002. A generalized approach to parameterizing convection combining ensemble and data assimilation techniques. Geophysical Research Letters 29, doi:10.1029/2002GL015311.

Hack, J. J., B. A. Boville, B. P. Briegleb, J. T. Kiehl, P. J. Rasch, and D. L. Williamson, 1993: Description of the NCAR Community Climate Model (CCM2). NCAR Technical Note, NCAR/TN-382+STR

Hanna, S.R., Lu, Z., Frey, H.C., Wheeler, N., Vukovich, J., Arunachalam, S., Fernau, M., Hansen, D.A., 2001. Uncertainties in predicted ozone concentrations due to input uncertainties for the UAM-V photochemical grid model applied to the July 1995 OTAG domain. Atmospheric Environment 35, 891-903.

Hogrefe, C., Rao, S.T., Kasibhatla, P., Kallos, G., Tremback, C.J., Hao, W., Olerud, D., Xiu, A., McHenry, J., Alapaty, K., 2001. Evaluating the performance of regional-scale photochemical modeling systems: Part I - Meteorological predictions. Atmospheric Environment 35, 4159-4174.

Hogrefe, C. W. Hao, K. Civerolo, J.-Y. Ku, R.S. Gaza, L. Sedefian, G. Sistla, K. Schere, A. Gilliland, and R. Mathur, Daily Photochemical Simulations of Ozone and Fine Particulates Over New York State: Findings and Challenges, J. Appl. Meteor., 46, 961–979, 2007.

Hong, S.-Y., and H.-L. Pan, 1996: Nonlocal boundary layer vertical diffusion in a medium-range forecast model. Mon. Wea. Rev., 124, 2322-2339.

Hong, S.-Y., Noh, Y., Dudhia, J., 2006. A new vertical diffusion package with an explicit treatment of entrainment processes. Monthly Weather Review 134, 2318-2341.

Honoré, C., Rouil, L., Vautard, R., Beekmann, M., Bessagnet, B., Dufour, A., Elichegaray, C., Flaud, J.-M., Malherbe, L., Meleux, F., Menut, L., Martin, D., Peuch, A., Peuch, V.-H., Poisson, N., 2008. Predictability of European air quality: The assessment of three years of operational forecasts and analyses. J. Geophys. Res., 113, D04301, doi:10.1029/2007JD008761.

Lacono, M.J., Delamere, J.S., Mlawer, E.J., Shephard, M.W., Clough, S.A., Collins, W.D., 2008. Radiative forcing by long-lived greenhouse gases: Calculations with the AER radiative transfer models. Journal of Geophysical Research 113, D13103, doi:10.1029/2008JD009944.

IFS DOCUMENTATION - Cy31r1, Operational implementation 12 September 2006, PART IV: PHYSICAL PROCESSES. ECMWF, Reading, U.K., 2007. http://www.ecmwf.int/research/ifsdocs/CY31r1/PHYSICS/IFSPart4.pdf

Janjic, Zavisa I., 1990: The step-mountain coordinate: Physical package. Mon. Wea. Rev., 118, 1429-1443.

Janjic, Zavisa I., 1994: The step-mountain eta coordinate model: Further development of the convection, viscous sublayer, and turbulent closure schemes. Mon. Wea. Rev., 122, 927-945.

Kain, J.S., Fritsch, J.M., 1990. A one-dimensional entraining/detraining plume model and its application in convective parameterization. Journal of the Atmospheric Sciences 47, 2784-2802.

Kain, J.S., Fritsch, J.M., 1993. Convective parameterization for mesoscale models: The Kain–Fritsch scheme. *The Representation of Cumulus Convection in Numerical Models*, Meteorological Monograph No. 46, American Meteorological Society, Boston, 165–170.

Kain, J. S., 2004. The Kain-Fritsch convective parameterization: An update. Journal of Applied Meteorology 43, 170–181.

Li, J., Barker, H.W., 2005. A radiation algorithm with correlated k-distribution. Part I: Local thermodynamic equilibrium. Journal of the Atmospheric Sciences 62, 286-309.

Liu, G., Hogrefe, C. and S.T. Rao, 2003. Evaluating the performance of regional-scale meteorological models:effect of clouds simulation on temperature prediction. Atmospheric Environment, 37, 1425-1433.

Majewski, D., Liermann, D., Prohl, P., Ritter, B., Buchhold, M., Hanisch, T., Paul, G., Wergen, W., Baumgardner, J., 2002. The operational global icosahedral-hexagonal gridpoint model GME: Description and high-resolution tests. Monthly Weather Review 130, 319–338.

Matthias, Volker, Builtjes, Peter, Chemel, Charles, Friese, Elmar, Galmarini, Stefano, Pérez, Juan L., Prank, Marje, Quante, Markus, Schlünzen, K. Heinke, San Jose, Roberto, Sofiev, Mikhail, Stern, Rainer, Struzewska, Joanna, Vautard, Robert, Wolke, Ralf: Comparative analysis of chemistry transport simulations of a particulate matter episode over Germany, International Aerosol Conference, Helsinki, 29.8. – 3.9. 2010.

McHenry, J.N., Ryan, W.F., Seaman, N.L., Coats Jr., C.J., Pudykiewicz, J., Arunachalam, S., Vukovich, J.M., 2004. A real-time Eulerian photochemical model forecast system. Bulletin of the American Meteorological Society 85, 525-548.

McKeen, S., Wilczak, J., Grell, G., Djalalova, I., Peckham, S., Hsie, E.-Y., Gong, W., Bouchet, V., Ménard, S., Moffet, R., McHenry, J., McQueen, J., Tang, Y., Carmichael, G.R., Pagowski, M., Chan, A., Dye, T., 2005. Assessment of an ensemble of seven real-time ozone forecasts over Eastern North America during the summer of 2004. Journal of Geophysical Research 110, D21307, doi:10.1029/2005JD005858, 16 pp.

Mlawer, E.J., Taubman, S.J., Brown, P.D., Lacono, M.J., Clough, S.A., 1997. RRTM, a validated correlated-k model for the longwave. Journal of Geophysical Research 102, 16663-16682.

Monks, P. S., C. Granier, S. Fuzzi, A. Stohl, M. Williams, H. Akimoto, M. Amman, A.Baklanov, U. Baltensperger, I. Bey, N. Blake, R.S. Blake, K. Carslaw, O.R. Cooper, F. Dentener, E. Fragkou, G. Frost, S. Generoso, P. Ginoux, V. Grewe, A. Guenther, H.C., Hansson, S. Henne, J. Hjorth, A. Hofzumahaus, H. Huntrieser, M.E. Jenkin, J. Kaiser, M. Kanakidou, Z. Klimont, M. Kulmala, M.G. Lawrence, J.D. Lee, C. Liousse, G. McFiggans, A. Metzger, A. Mieville, N. Moussiopoulos, J.J. Orlando, P.I. Palmer, D. Parrish, A. Petzold, U. Platt, U. Poeschl, A.S.H. Prévôt, C.E. Reeves, S. Reiman, Y. Rudich, K. Sellegri, R. Steinbrecher, D. Simpson, H. ten Brink, J. Theloke, G. van der Werf, R. Vautard, V. Vestreng, Ch. Vlachokostas, R. vonGlasow, 2009, Atmospheric composition change – global and regional air quality, Atmospheric Environment, 43, 5268-5350.

Morrison, H., Thompson, G., Tatarskii, V., 2009. Impact of cloud microphysics on the development of trailing stratiform precipitation in a simulated squall line: Comparison of one- and two-moment schemes. Monthly Weather Review 137, 991-1007.

Noilhan, J., Planton, S., 1989. A simple parameterization of land surface processes for meteorological models. Monthly Weather Review 117, 536–549.

Otte, T.L., Pouliot, G., Pleim, J.E., Young, J.O., Schere, K.L., Wong, D.C., Lee, P.C.S., Tsidulko, M., McQueen, J.T., Davidson, P., Mathur, R., Chuang, H.-Y., DiMego, G., Seaman, N.L., 2005. Linking the

Eta Model with the Community Multiscale Air Quality (CMAQ) modeling system to build a national air quality forecasting system. Weather and Forecasting 20, 367-384.

Otte, T.L., 2008. The impact of nudging in the meteorological model for retrospective air quality simulations. Part I: Evaluation against national observation networks. Journal of Applied Meteorology and Climatology 47, 1853–1867.

Pielke, R.A., Uliasz, M., 1998. Use of meteorological models as input to regional and mesoscale air quality models – limitations and strengths. Atmospheric Environment 32, 1455-1466.

Pirovano, G., I. Coll, M. Bedogni, S. Alessandrini, M.P. Costa, V. Gabusi, F. Lasry, L. Menut, R. Vautard, 2007: On the influence of meteorological input on photochemical modelling of a severe episode over a coastal area. Atmospheric Environment, 41, 6445-6464.

Pleim, J.E., Xiu, A., 2003: Development of a land-surface model. Part II: Data assimilation. Journal of Applied Meteorology, 42, 1811–1822.

Pleim, J.E., 2007a. A combined local and nonlocal closure model for the atmospheric boundary layer. Part I: model description and testing. Journal of Applied Meteorology and Climatology 46, 1383–1395.

Pleim, J.E., 2007b. A combined local and nonlocal closure model for the atmospheric boundary layer. Part II: application and evaluation in a mesoscale meteorological model. Journal of Applied Meteorology and Climatology 46, 1396–1409.

Pleim J.E., Gilliam, R., 2009. An indirect data assimilation scheme for deep soil temperature in the Pleim-Xiu land surface model. Journal of Applied Meteorology and Climatology 48, 1362-1376.

Pudykiewicz, J., Benoit, R., Mailhot, J., 1992. Inclusion and verification of a predictive cloud water scheme in a regional weather prediction model. Monthly Weather Review 120, 612–626.

Rao, S.T., Galmarini, S., Puckett, K., 2011. Air Quality Model Evaluation International Initiative (AQMEII): Advancing the state of the science in regional photochemical modeling and its applications. Bulletin of the American Meteorological Society 92, 23-30.

Reisner, J., Rasmussen, R.M., Bruintjes, R.T., 1998. Explicit forecasting of supercooled liquid water in winter storms using the MM5 mesoscale model. Quarterly Journal of the Royal Meteorological Society 124 B, 1071-1107.

Ritter, B., Geleyn, J.-F., 1992. A comprehensive radiation scheme for numerical weather prediction models with potential applications in climate simulations. Monthly Weather Review 120, 303-325.

Rockel, B; Will, A; Hense, A, 2008. The Regional Climate Model COSMO-CLM(CCLM), Meteorologische Zeitschrift, 17, 4, 347-348.

Sass, B.H., Rontu, L., Raisanen, P., 1994. HIRLAM-2 radiation scheme: Documentation and tests. HIRLAM Technical Report No. 16. [Available from: http://hirlam.org/publications/TechReports/index.html].

Schättler, U., Doms, G., Schraff, C., 2009. A description of the nonhydrostatic regional COSMO-Model. Part VII: User's guide. Deutscher Wetterdienst, Offenbach, 2009 [available from http://www.cosmo-model.org].

Schrodin, R., Heise, E., 2001. The Multi-Layer Version of the DWD Soil Model TERRA-LM, COSMO Technical Report No. 2, Offenbach.

Seaman, N.L., 2000. Meteorological modeling for air-quality assessments. Atmospheric Environment 34, 2231-2259.

Seibert, P., Beyrich, F., Gryning, S.-E., Joffre, S., Rasmussen, A., and Tercier, Ph.: Review and intercomparison of operational methods for the determination of the mixing height, Atmos. Environ., 34, 1001-1027, doi:10.1016/S1352-2310(99)00349-0, 2000.

Seifert A. and K.D. Beheng, 2001. A double-moment parameterization for simulating autoconversion, accretion and selfcollection. Atmospheric Research 59–60, 265–281.

Seifert, A., and S. Crewell, 2008: A revised cloud microphysical parameterization for operational numerical weather prediction using the COSMO model. Proc. 15th International Conference on Clouds and Precipitation. Cancun, Mexico.

Sistla, G., Zhou, N., Hao, W., Ku, J.-Y., Rao, S.T., Bornstein, R., Freedman, F., Thunis, P., 1996. Effects of uncertainties in meteorological inputs on Urban Airshed Model predictions and ozone control strategies. Atmospheric Environment 30, 2011-2025.

Skamarock, W. C., Klemp, J. B., Dudhia, J., Gill, D. O., Barker, D. M., Duda, M. G., Huang, X.-Y., Wang, W., Powers, J. G., 2008. *A description of the Advanced Research WRF Version 3*. Technical Note NCAR/TN-475+STR, National Center for Atmospheric Research, Boulder, Colorado, 113 pp. [Available from www.mmm.ucar.edu/wrf/users/docs/arw_v3.pdf]

Smyth, S., Yin, D., Roth, H., Jiang, W., Moran, M.D., Crevier, L.-P., 2006. The impact of GEM and MM5 meteorology on CMAQ air quality modeling results in eastern Canada and the northeastern United States. Journal of Applied Meteorology 45, 1525–1541, DOI: 10.1175/JAM2420.1.

Steppeler, J., Doms, G., Schättler, U., Bitzer, H.W., Gassmann, A., Damrath, U., Gregoric, G., 2003. Meso-gamma scale forecasts using the nonhydrostatic model LM. Meteorology and Atmospheric Physics 107, 4576, doi:10.1007/s00703-001-0592-9, 75–96.

Stern, R., P. Builtjes, M. Schaap, R. Timmermans, R. Vautard, A. Hodzic, M. Memmesheimer, H. Feldmann, E. Renner, R. Wolke, and A. Kerschbaumer, 2008 : A model inter-comparison study focusing on episodes with elevated PM10 concentrations. Atmos. Environ, 42, 4567-4588.

von Storch, H; Langenberg, H; Feser, F, 2000. A spectral nudging technique for dynamical downscaling purposes. Monthly Weather Review 128, 10, 3664-3673.

Struzewska, J., Kaminski, J.W., 2008. Formation and transport of photooxidants over Europe during the July 2006 heat wave - Observations and GEM-AQ model simulations. Atmospheric Chemistry and Physics 8, 721-736.

Tarasick, D.W., Moran, M.D., Thompson, A.M., Carey-Smith, T., Rochon, Y., Bouchet, V.S., Gong, W., Makar, P.A., Stroud, C., Ménard, S., Crevier, L.-P., Cousineau, S., Pudykiewicz, J.A., Kallaur, A., Moffet, R., Ménard, R., Robichaud, A., Cooper, O.R., Oltmans, S.J., Witte, J.C., Forbes, G., Johnson, B.J., Merrill, J,. Moody, J.L., Morris, G., Newchurch, M.J., Schmidlin, F.J., Joseph, E., 2007. Comparison of Canadian air quality forecast models with tropospheric ozone profile measurements above mid-latitude North America during the IONS/ICARTT campaign: Evidence for stratospheric input. Journal of Geophysical Research 112, D12S22, doi: 10.1029/2006JD007782.

Taylor, K.E., 2001. Summarizing multiple aspects of model performance in a single diagram. J. Geophys. Res. 106 (D7), 7183–7192.

Tiedtke, M., 1989. A comprehensive mass flux scheme for cumulus parameterization in large-scale models. Mon. Wea. Rev., 117, 1779-1799.

Tremblay, A., 2005. The stratiform and convective components of surface precipitation. Journal of the Atmospheric Sciences 62, 1513-1528.

Tsyro, S., Støren, E., 1999. New meteorological model for air pollution transport models. EMEP/MSC-W Note 3/99, July 1999.

Tustison, B., Harris, D., Foufoula-Georgiou, E., 2001. Scale issues in verification of precipitation forecasts. Journal of Geophysical Research 106, 11775-11784.

Wang, X., Zhang, L., Moran, M.D., 2010. Uncertainty assessment of current size-resolved parameterizations for below-cloud particle scavenging by rain. Atmospheric Chemistry and Physics 10, 5685-5705, doi:10.5194/acp-10-5685-2010.

Xiu, A., Pleim, J.E., 2001. Development of a land-surface model. Part I: Application in a mesoscale meteorological model. Journal of Applied Meteorology 40, 192-209.

Yiou, P., Vautard, R., Naveau, P., Cassou, C., 2007. Inconsistency between atmospheric dynamics and temperatures during the exceptional 2006/2007 fall/winter and recent warming in Europe. Geophysical Research Letters 34, L21808, doi:10.1029/2007GL031981.

Zhang, F., Bei, N., Nielsen-Gammon, J.W., Li, G., Zhang, R., Stuart, A., Aksoy, A., 2007. Impacts of meteorological uncertainties on ozone pollution predictability estimated through meteorological and photochemical ensemble forecasts. Journal of Geophysical Research 112, art. no. D04304,

Figure Captions

Figure 1: Seasonal 850 hPa temperature anomalies (K) for 2006.

Figure 2: Seasonal 500 hPa geopotential height anomalies (dam) for 2006.

Figure 3: Six subregions selected for model and observation comparisons: (left panel) North America (24°N-54°N, 130°W-60°W); (right panel) Europe (30°N-70°N;15°W-30°E). The exact subregion boundaries are the following: (1) NA1, 31°N-42°N, 125°W-112°W; (2) NA2, 25°N-37°N, 104°W-90°W; (3) NA3, 36.5°N-48.5°N, 85°W-69°W; (4) EU1, 42°N-60°N, 10°W-5°E; (5) EU2, 46°N-56°N, 5°E-25°E; and (6) EU3, 43°N-46°N, 7°E-15°E. Dots indicate the location of the observation stations considered in this study. Sites used for profile calculations, where ozone soundings are launched are marked with a "+" sign.

Figure 4: Monthly averages of subregional mean wind speeds as observed (thick solid black lines) and as simulated from the various meteorological models used in AQMEII.

Figure 5: Mean annual diurnal cycle of wind speed by subregion as observed (thick solid black lines) and as simulated from the various meteorological models used in AQMEII.

Figure 6: Taylor plots for the simulation of daily wind speed over each continent (left panel: NA; right panel: EU). Each symbol type stands for a subregion. The amplitude of variability is the radial distance to origin. The amplitude of observation for a given subregion is shown by the symbol on the x axis. Larger symbols indicate the skill of the ensemble mean (open symbol) and the ensemble median (solid symbol).

Figure 7/ Spatial distribution of the mean annual wind speed at 10 m as observed at measurement sites and simulated over the two continents by WRF for North America and MM5 for Europe.

Figure 8: Comparison of vertical profiles of wind speed for NA and EU soundings. The observations are based on irregular ozone soundings at six stations for EU and six stations for NA. The statistical

parameters bias, root mean square error and correlation were derived for time series in given altitudes.

Figure 9: Annual times series of PBL heights at Lindenberg, Germany, derived from radiosondes (obs) and from two selected models at 12UTC and 18 UTC.

Figure 10: Simulated and observed monthly mean 2-m temperature values for the six subregions.

Figure 11: Same as Figure 5 for the mean diurnal cycle of 2-m temperature.

Figure 12: same as Figure 8 but for temperature profiles

Figure 13: Simulated vs. observed 99.5th centiles of area-average hourly temperature distributions for each continental subregion of Figure 3. Each point represents a model and each color a different subregion. The area names are indicated on the figure.

Figure 14: Left panels: Seasonal cycle of relative humidity (%) at 2 m as averaged over observations (thick black line) or model simulations (other lines) for three NA subregions; Right panels: As in left panels for hourly precipitation rate (in mm).

Figure 15: Same as Figure 8 but for Relative humidity

Figure 16: Left panels: Mean monthly mid-day (hours 10-14 local time) surface shortwave radiation (W m^{-2}) predicted by four meteorological models at center points of three NA subregions [NA1: 36.5°N, 118.5°W; NA2: 31°N, 97°W; NA3: 42.5°N, 77°W]; Right panels: Same plots for nine models and center points of three EU subregions [EU1: 51°N, 2.5°W; EU2: 51°N, 15°E; EU3: 44.5°N, 11°E].

Figure 17: Left panels**:** Mean annual diurnal cycle (UTC) of surface shortwave radiation (W m^{-2}) predicted by four meteorological models at center points of three NA subregions [NA1: 36.5°N, 118.5°W; NA2: 31°N, 97°W; NA3: 42.5°N, 77°W]; Right panels: Same but for nine models and center points of three EU subregions [EU1: 51°N, 2.5°W; EU2: 51°N, 15°E; EU3: 44.5°N, 11°E].

Figure 18: Same as Fig. 16 but for mean monthly standard deviation of hourly surface shortwave radiation (W m^{-2}) for mid-day period (hours 10-14 LT).

Figure 19: Histograms of percentage occurrence of observed and predicted hourly precipitation amount (mm h^{-1}) for the (a) winter and (b) summer season for the NA1 subregion, (c) winter and (d) summer season for the NA2 subregion, and (e) winter and (f) summer season for the NA3 subregion.

Figure 20: Spatial distribution of seasonal accumulated precipitation (mm) for the US1 WRF simulation and observations, which are represented by the Parameter-elevation Regressions on Independent Slopes Model (PRISM). Left panels represent winter (DJF) and right summer (JJA).

Research Group that operated simulations and processing	Model	Appx. horiz. resol. (km)	# of vertical levels; # of levels < 1 km; model top;	Key parameterizations LSM = Land Surface Model; PBL = Planetary Boundary Layer Scheme; MP = Microphysics Scheme; CuP = Cumulus Parameterization; LWR = Long-Wave Radiation Scheme	Analysis and initialization AI) , integration (IN), boundary conditions (BC), data assimilation (DA)
				North America	
Environment Canada (CA)	GEM (Côté et al., 1998a,b)	15 (0.1375°)	58 8 10 hPa	LSM: ISBA (Noilhan and Planton, 1989; Belair et al., 2003) PBL: TKE scheme (Belair et al., 2003) MP: Sundqvist (Pudykiewicz et al., 1992) CuP: KFC (Kain and Fritsch, 1990, 1993) LWR: Li and Barker (2005)	AI: Global 0.33° analysis every 6 h IN: 1.25 d segments with 0.25 d overlap BC: None (global variable grid) DA: None
Helmholtz-Zentrum Geesthacht (DE)	COSMO-CLM (Steppeler et al., 2003; Schättler et al., 2009, Rockel et al., 2008)	24	40 11 20 hPa	LSM: multi-layer model TERRA-LM (Grasselt et al., 2008) PBL: TKE closure, Doms and Schaettler, 2004,Doms et al., 2008 MP: Seifert and Beheng, 2001 CuP: Tiedtke, 1989 LWR: Ritter and Geleyn, 1992	AI: 1.875° NCEP1 reanalysis IN: continuous run, 1 month spin up time BC: same as AI DA: Spectral nudging of wind in higher altitudes (von Storch et al., 2000)
Univ. Aarhus (DK)	MM5	50	29 11 100 hPa	LSM: NOAH (Ek et al., 2003) PBL: Eta MY (Janjic, 1990, 1994) MP: mixed phase Reisner 1 (Reisner et al. 1998) CuP: BM (Betts and Miller, 1993) LWR: CCM2 (Hack et al., 1993)	AI/IN/DA: One continuous simulation with grid nudging FDDA using 1º NCEP-FNL global analysis every 6 h. Relaxation/inflow-outflow lateral BCs.
Univ. Aveiro (PT)	MM5 Dudhia, 1993; Grell et al., 1994)	27	23 15 100 hPa	LSM: Five-Layer Soil model (Dudhia, 1996) PBL: MRF (Hong and Pan, 1996) MP: Reisner 2 (Reisner et al., 1998) CuP: Grell and Devenyi (2002) LWR: RRTM (Lacono et al 2008)	AI: 1° NCEP-FNL global analysis every 6 h IN: 5.25 d segments with 0.25 d overlap BC: same as AI DA: Not used
Environmental Protection Agency (US)	WRF (Skamarock et al., 2008)	12	34 14 50 hPa	LSM: PX LSM (Xiu and Pleim, 2001; Pleim and Xiu, 2003) PBL: ACM2 (Pleim, 2007a,b) MP: Morrison et al. (2009) CuS: Kain-Fritsch2 (Kain, 2004)	AI: 12-km NAM analysis + radiosondes every 6 h IN: 5.5 d segments with 0.5 d overlap BC: same as AI DA: V, T, q nudging in atmosphere; T, q

				LWR: RRTMG (Lacono et al 2008)	nudging in soil
Europe					
IFT (DE)	COSMO (Steppeler et al., 2003; Schättler et al., 2009)	24	40 total 9 below 1 km	LSM: multi-layer model TERRA-ML (Grasselt et al. 2008) PBL: prognostic TKE, 2.5 closure scheme (Doms et al. 2008) MP: Kessler type bulk scheme, ice phase, prognostic precipitation (Doms et al. 2007; Seifert and Crewell, 2008) CuP: mass flux scheme of Tiedke (1989) LWR: ∂-two-stream (Ritter and Geleyn 1992)	Initialization and boundary conditions from the GME system (Majewski et al. 2002)
IMK-IFU (DE)	WRF/Chem	22.5	36 total 13 below 1 km	LSM: NOAH (Chen and Dudhia 2001, Ek et al, 2003) LWR: RRTM (Mlawer et al., 1997) CuP: Grell (Grell and Devenyi 2002) PBL : Hong et al. (2006)	Initialization and nudging from NCEP GFS 1° analyses. Nudging above PBL detailed in Gilliam and Pleim (2010). Note: the run was done with aerosol radiation effects (direct and indirect) and also included some aqueous chemical reactions (see Forkel et al., in preparation in this issue).
Helmholtz-Zentrum Geesthacht (DE)	COSMO-CLM (Steppeler et al., 2003; Doms and Schättler, 2004, Rockel et al., 2008)	24	40 11 20 hPa	LSM: Multi-layer model TERRA-LM (Grasselt et al., 2008) PBL: TKE closure, Doms and Schaettler, 2004 MP: Seifert and Beheng, 2001 CuP: Tiedtke, 1989 LWR: Ritter and Geleyn, 1992	AI: 1.875° NCEP1 reanalysis IN: continuous multidecadal run BC: same as AI DA: Spectral nudging of wind in higher altitudes (von Storch et al., 2000)
Univ. Aarhus (DK)	MM5	50	29 11 100 hPa	LSM: NOAH (Ek et al., 2003) PBL: Eta MY (Janjic, 1990, 1994) MP: mixed phase Reisner 1 (Reisner et al. 1998) CuP: BM (Betts and Miller, 1993) LWR: CCM2 (Hack et al., 1993)	AI/IN/DA: One continuous simulation with grid nudging FDDA using 1º NCEP-FNL global analysis every 6 h. Relaxation/inflow-outflow lateral BCs.
FMI	ECMWF IFS	25	4 2 3.5 km	Physics from the IFS forecasting / assimilation system, interpolated to the grid (IFS, 2007)	ECMWF operational global forecasts
TNO	ECMWF IFS	25 (0.5^ox0.25^o)	4 2 3.5 km	Physics from the IFS forecasting / assimilation system, interpolated to the grid (IFS, 2007)	ECMWF operational global forecasts
IPSL	MM5 Dudhia, 1993; Grell et al., 1994)	20	32 9 100 hPa	LSM: NOAH (Ek et al., 2003) CuP: Grell and Devenyi (2002) LWR: RRTM (Mlawer et al., 1997) PBL: MRF PBL scheme	BC, initial conditions and nudging from ECMWF analyses

				MP: Reisner 2 (Reisner et al., 1998)	
Univ. Aveiro	MM5 Dudhia, 1993; Grell et al., 1994)	27	23 14 100 hPa	LSM: Five-Layer Soil model (Dudhia, 1996). CuP: Grell and Devenyi (2002) LWR: RRTM (Mlawer et al., 1997) PBL: MRF PBL scheme MP: Reisner 2 (Reisner et al., 1998)	
Univ. Hertfordshire (UK)	WRF (Skamarock et al., 2008)	18	**52** total **11** below 1 km	LSM: NOAH (Ek et al., 2003) PBL: Hong et al (2006) Microphysics Morrison et al (2009) CuP Grell and Devenyi (2002) LWR: RRTMG (Lacono et al 2008)	BC, initial conditions and nudging from ECMWF analyses
MSC (HR)	PARLAM-PS Tsyro and Støren 1999	50	**20** total **2** below 1 km	Most parameterizations from the HIRLAM model, see description in Sass et al (1994)	BC from ECMWF analyses, then forecasts 4x a day
NOAA	WRF/Chem	22.5	**36** total **13** below 1 km	LWR: RRTM (Mlawer et al., 1997) CuP: Grell (Grell and Devenyi 2002) LSM: NOAH (Chen and Dudhia 2001, Ek et al, 2003) PBL : Hong et al. (2006)	Initialization and nudging from NCEP GFS 1° analyses. Nudging above PBL detailed in Gilliam and Pleim (2010)

Table 1: Summary of some key characteristics of the meteorological models or model configurations participating in AQMEII.

Hour (UTC)	Mean Obs	M1EU	M2EU	M3EU	M4EU	M5EU	M7EU	M8EU	M9EU	M10EU
Bias (m)										
All hours	628	30	39	-476	-210	-3	-139	-361	-288	-55
0	363	11	34	-326	-246	22	-113	-317	-293	54
6	366	8	76	-326	-132	32	-126	-313	-276	29
12	1078	167	237	-612	72	33	-264	-280	-150	-170
18	705	-68	-193	-638	-538	-99	-52	-532	-434	-134
RMSE (m)										
All hours		542	464	645	481	358	386	538	471	433
0		443	223	403	310	208	215	394	343	281
6		547	253	412	271	206	209	400	343	253
12		550	589	797	410	402	504	527	478	536
18		615	631	836	768	514	503	750	650	565
Correlation										
All hours		0,66	0,70	0,56	0,70	0,78	0,77	0,69	0,76	0,62
0		0,41	0,78	0,03	0,59	0,85	0,73	0,09	0,73	0,56
6		0,27	0,69	-0,02	0,45	0,80	0,76	0,02	0,61	0,57
12		0,72	0,73	0,53	0,81	0,79	0,72	0,75	0,78	0,58
18		0,51	0,25	0,19	0,25	0,49	0,67	0,39	0,50	0,35

Table 2: Comparison of simulated PBL heights with observations at Lindenberg, at 0, 6, 12 and 18 UTC, and for all hours. On total, 1457 values were taken into account.

Region	Season	N	Obs	M1NA	M2NA	M3NA	M4NA	M5NA	Ensemble
NA1	DJF	115	93	130	66	158	135	206	139
NA1	JJA	115	16	9	2	37	22	30	20
NA2	DJF	203	106	137	143	123	132	195	146
NA2	JJA	203	125	283	99	274	290	258	241
NA3	DJF	291	152	186	207	194	184	235	201
NA3	JJA	291	208	431	418	314	351	440	391

Table 3: Observed and model-predicted 2006 mean seasonal precipitation accumulations at available measurement stations (mm) in three North American analysis subregions. The "Ensemble" column corresponds to mean of model values.

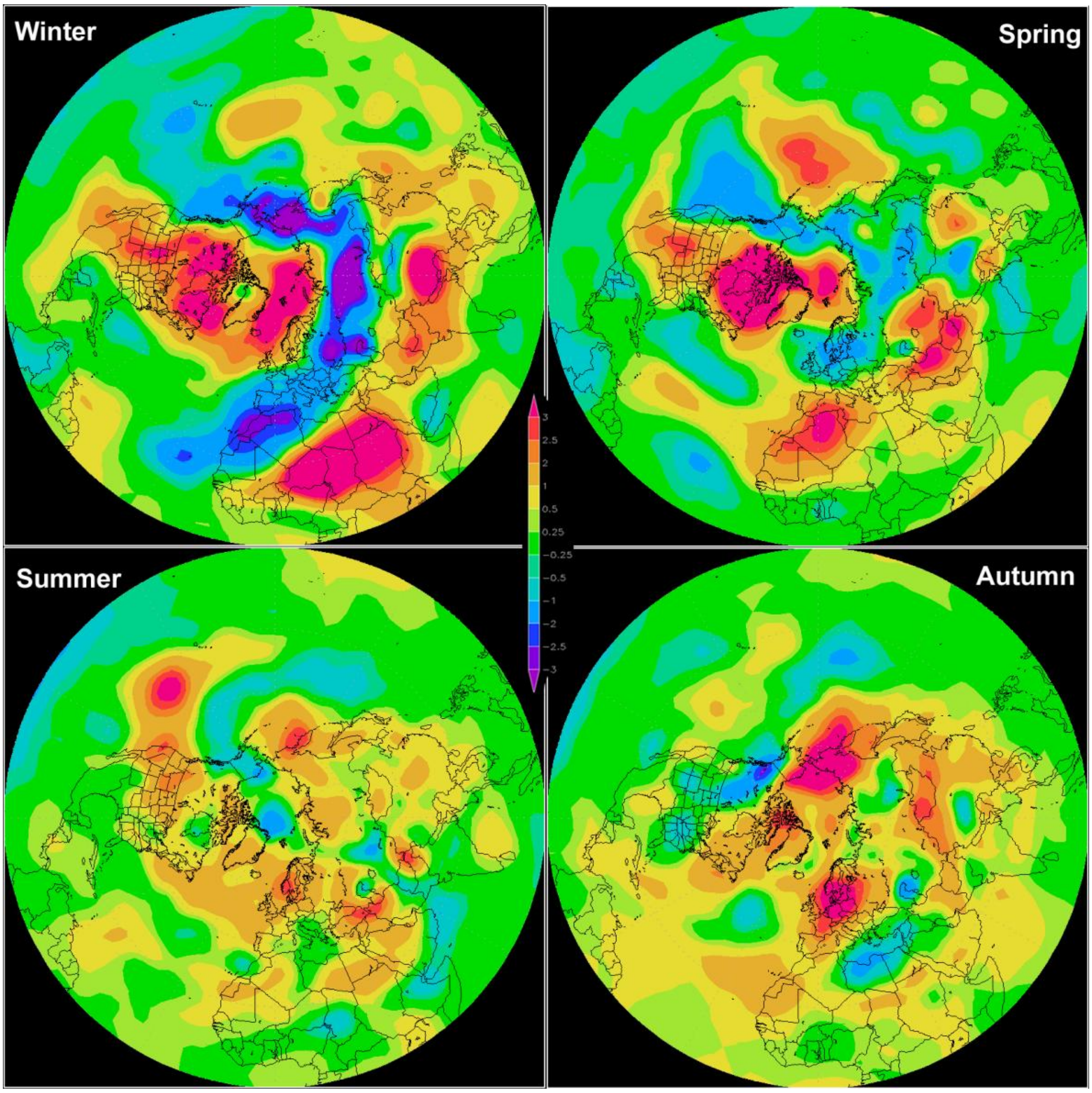

Figure 1

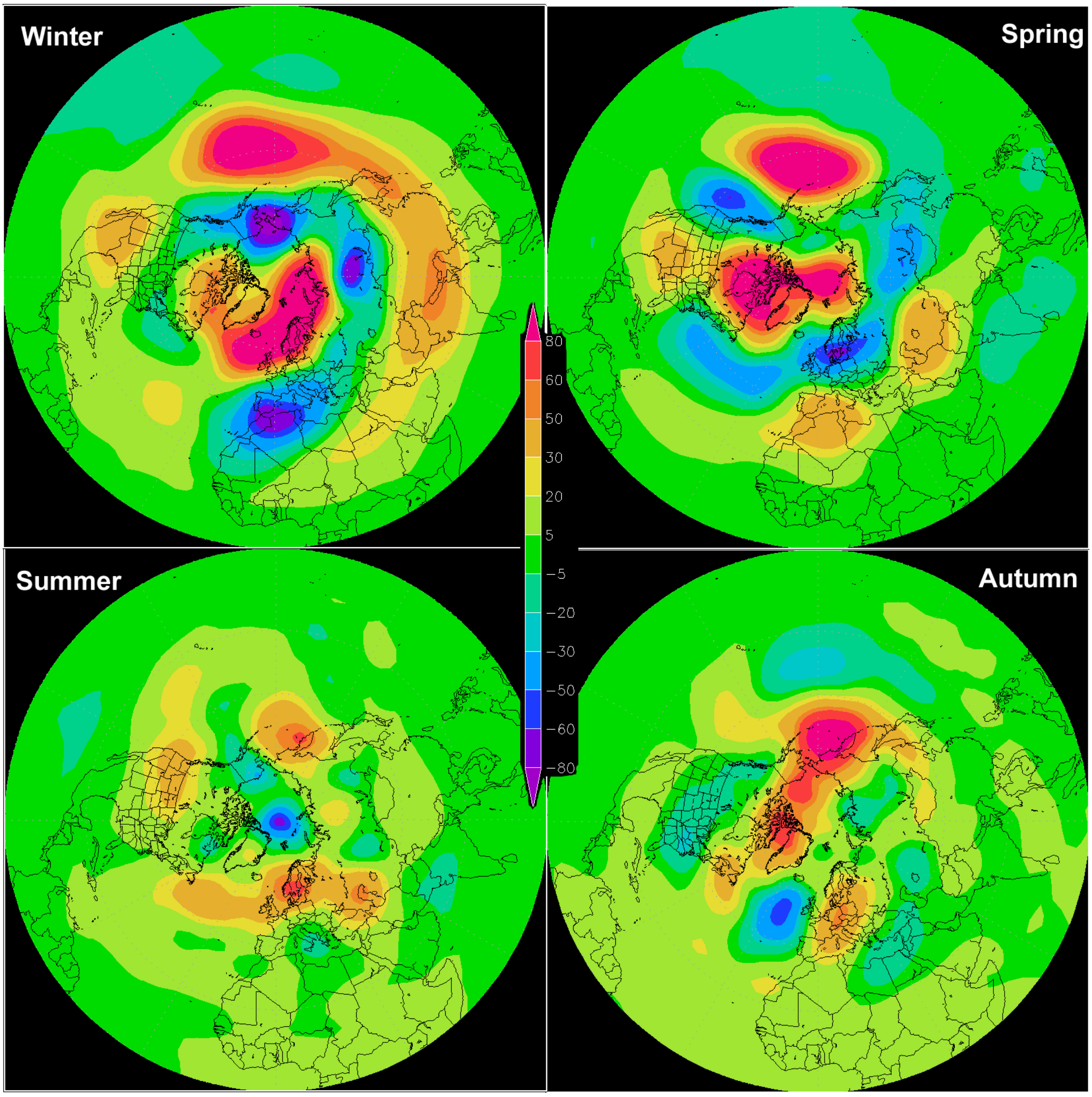

Figure 2

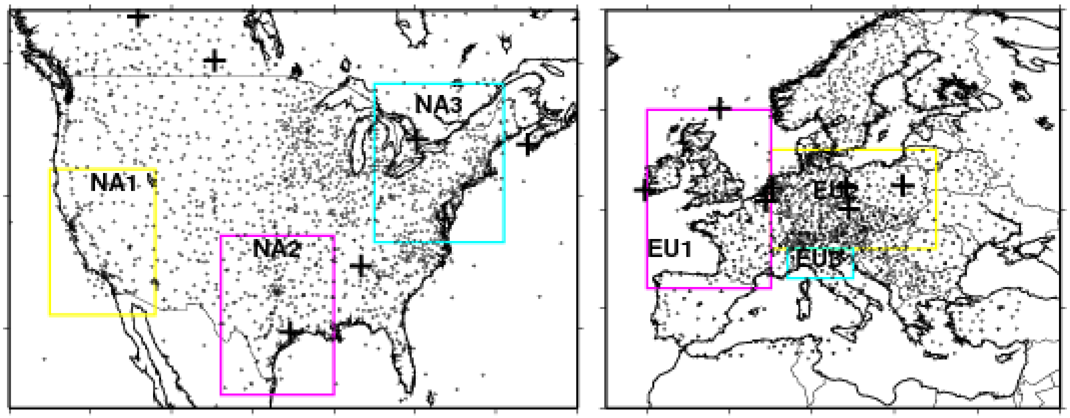

Figure 3

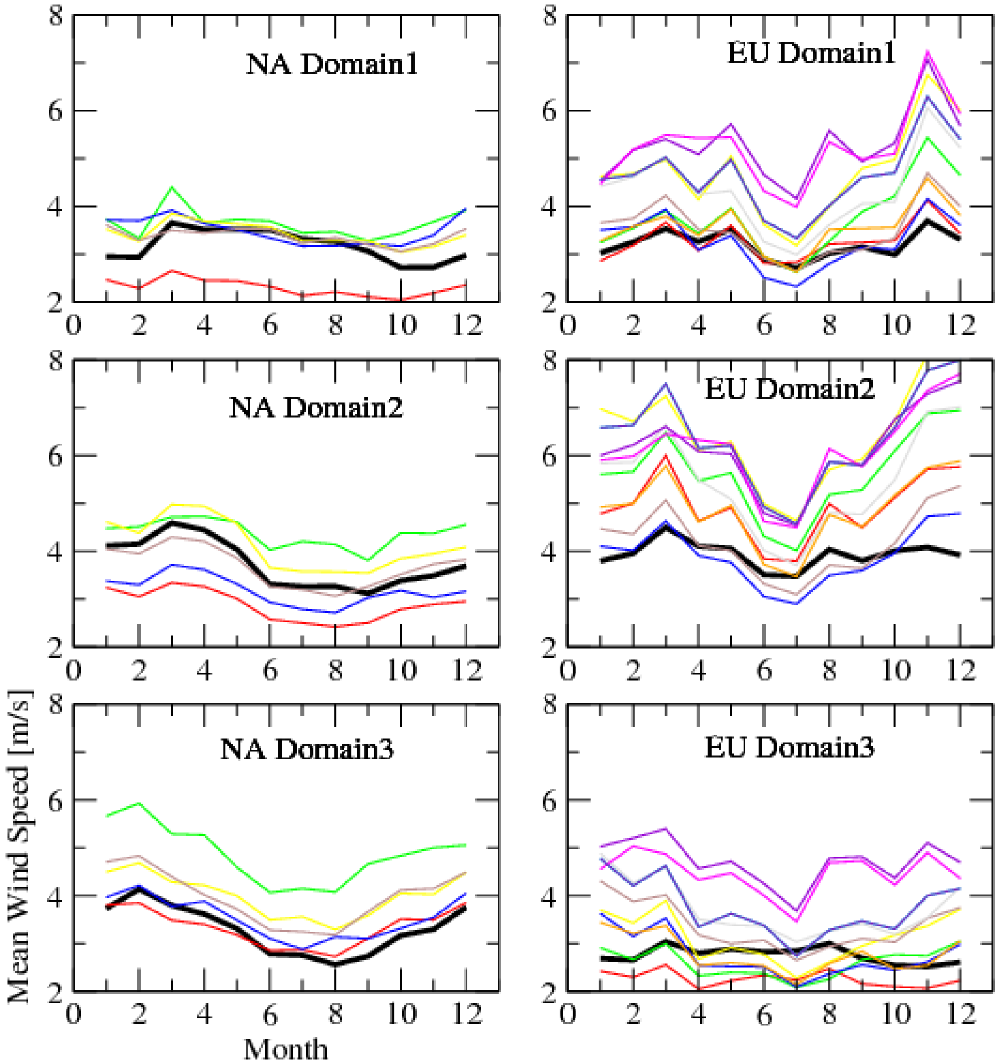

NA Domain1
EU Domain1
NA Domain2
EU Domain2
NA Domain3
EU Domain3
Mean Wind Speed [m/s]
Month

Figure 4

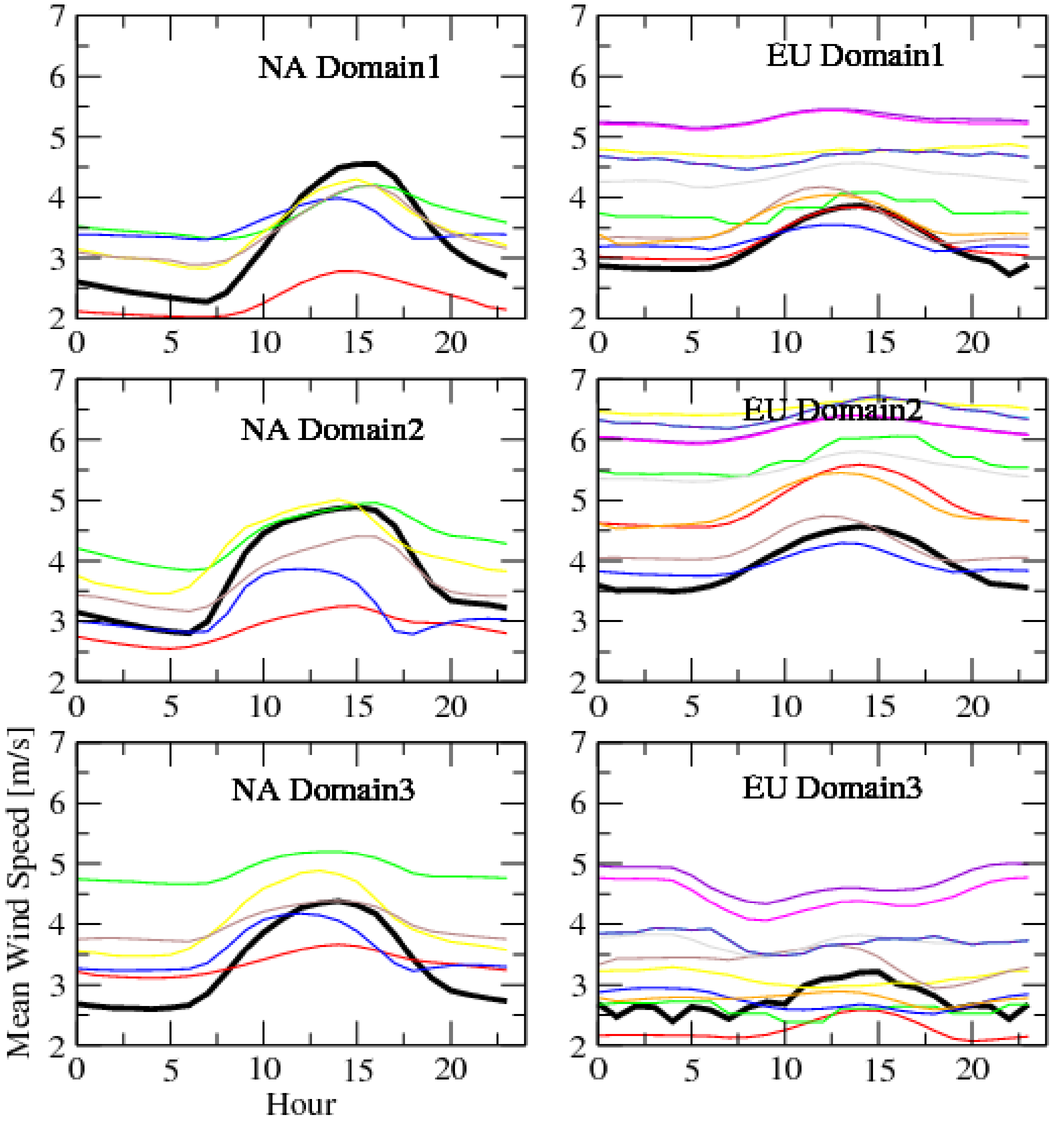

NA Domain1
EU Domain1
NA Domain2
EU Domain2
NA Domain3
EU Domain3
Mean Wind Speed [m/s]
Hour
7
6
5
4
3
2
0
5
10
15
20

Figure 5

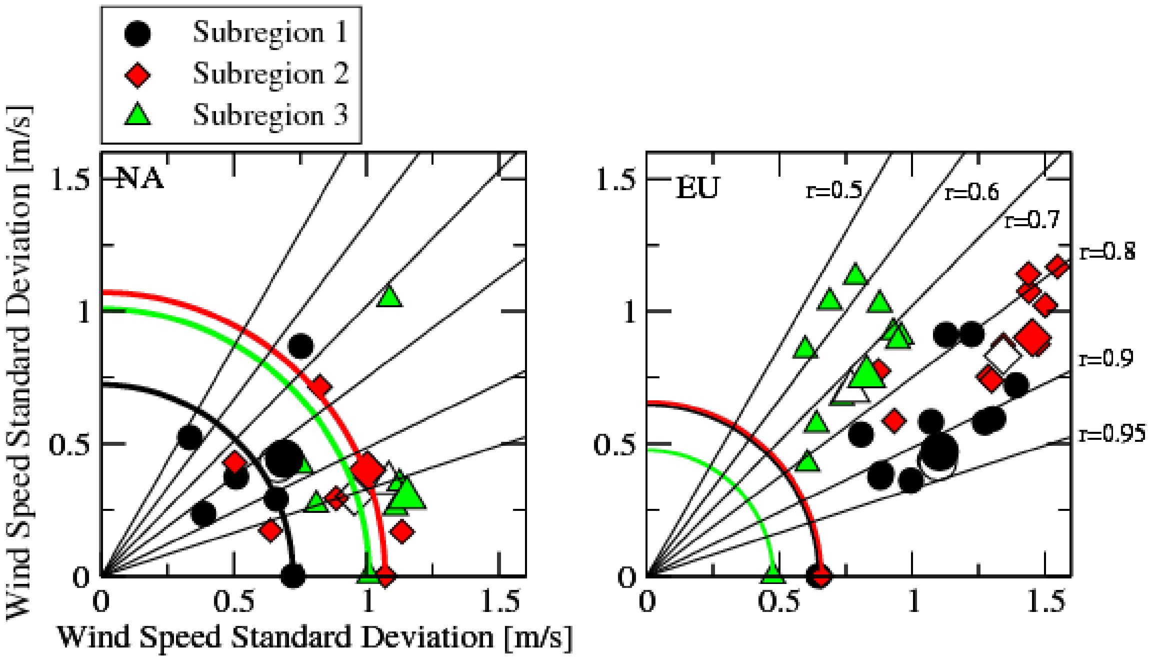

Figure 6

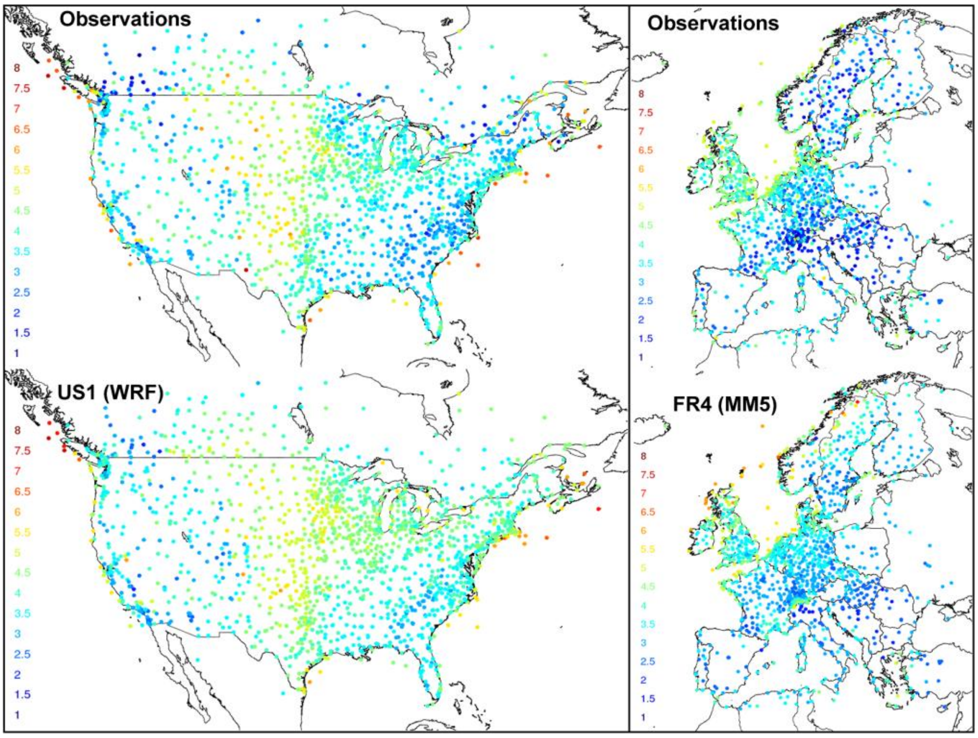

Figure 7

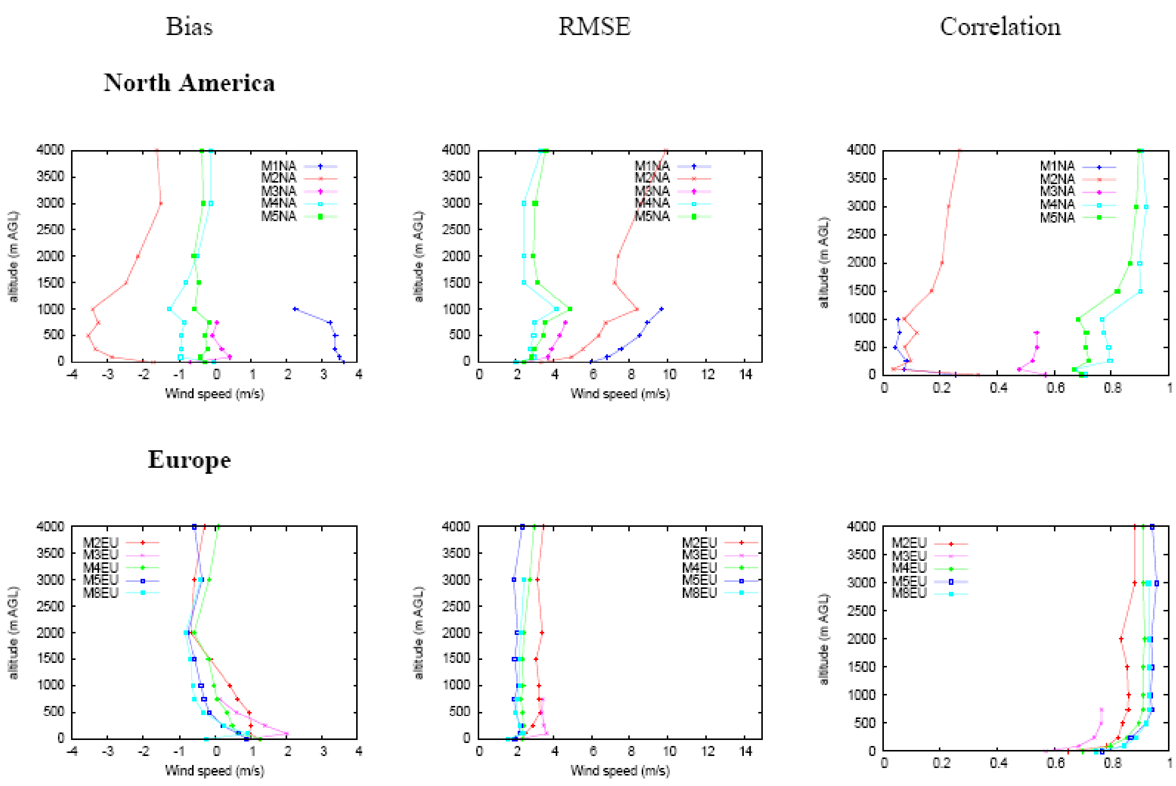

Figure 8

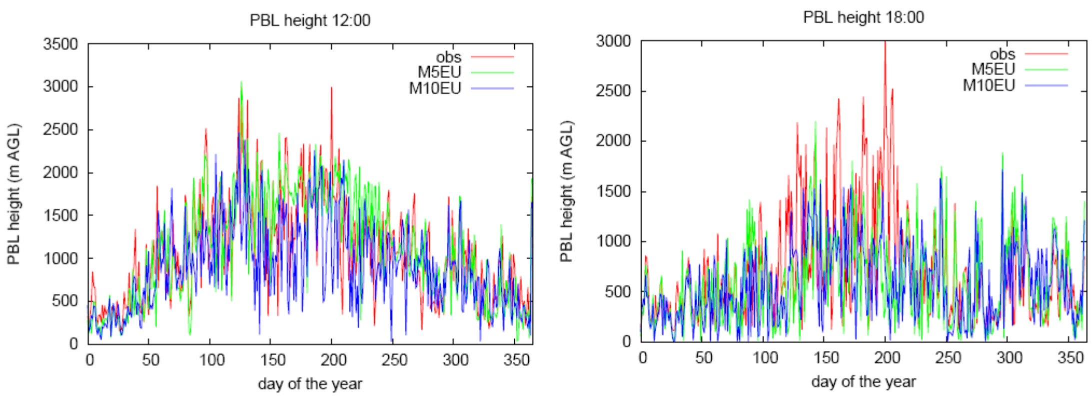

Figure 9

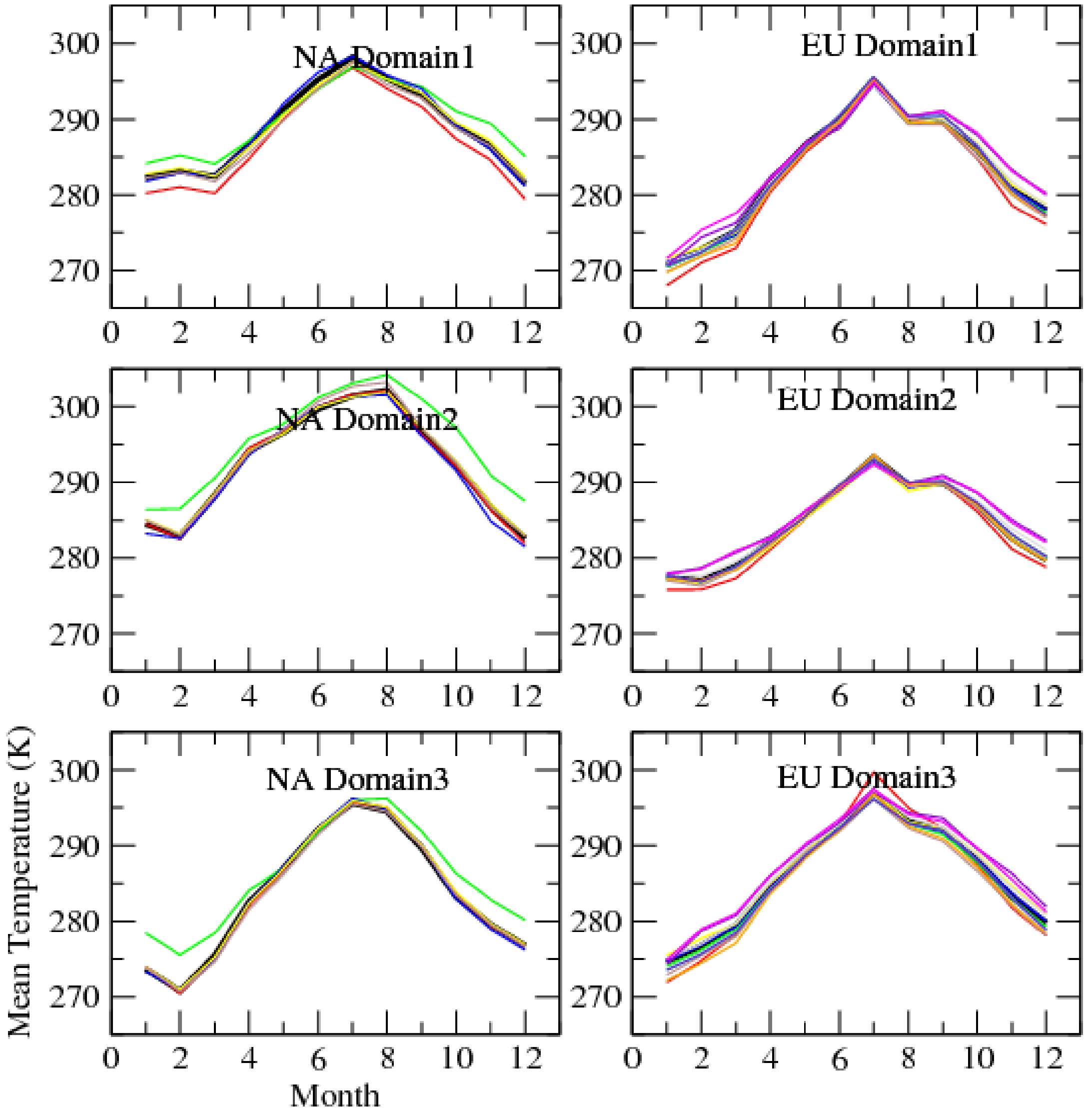
NA Domain1
EU Domain1
NA Domain2
EU Domain2
NA Domain3
EU Domain3
Mean Temperature (K)
Month
300
290
280
270
0
2
4
6
8
10
12

Figure 10

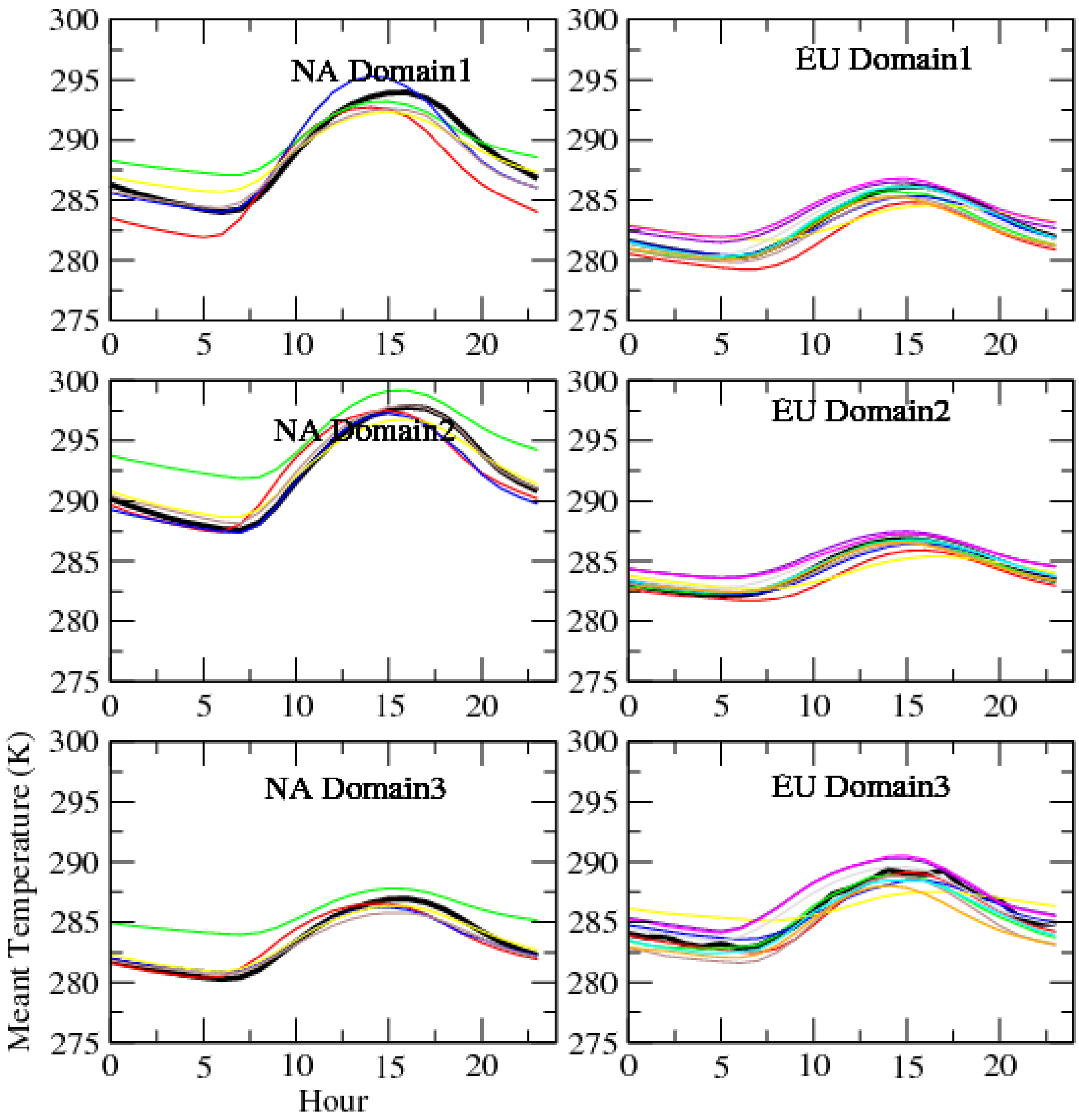
NA Domain1
EU Domain1
NA Domain2
EU Domain2
NA Domain3
EU Domain3
Meant Temperature (K)
Hour
300
295
290
285
280
275
0
5
10
15
20

Figure 11

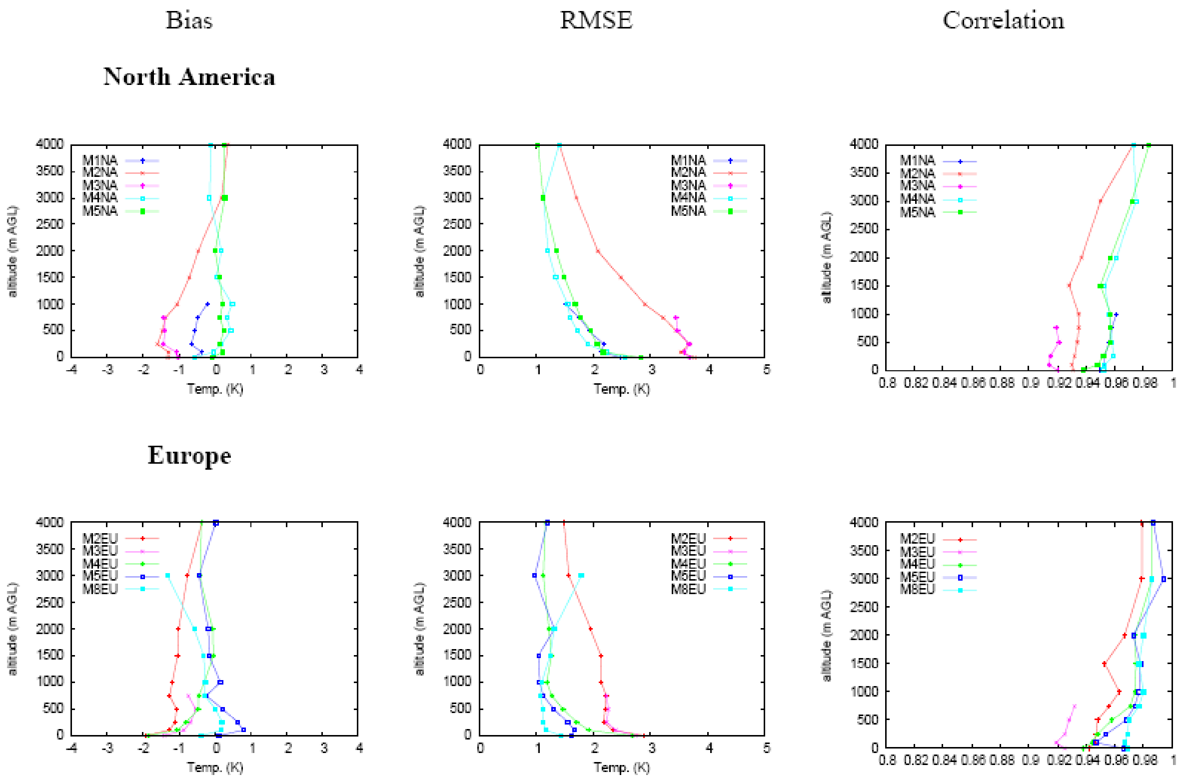
Bias
RMSE
Correlation
North America
Europe
M1NA
M2NA
M3NA
M4NA
M5NA
M2EU
M3EU
M4EU
M5EU
M8EU
altitude (m AGL)
Temp. (K)

Figure 12

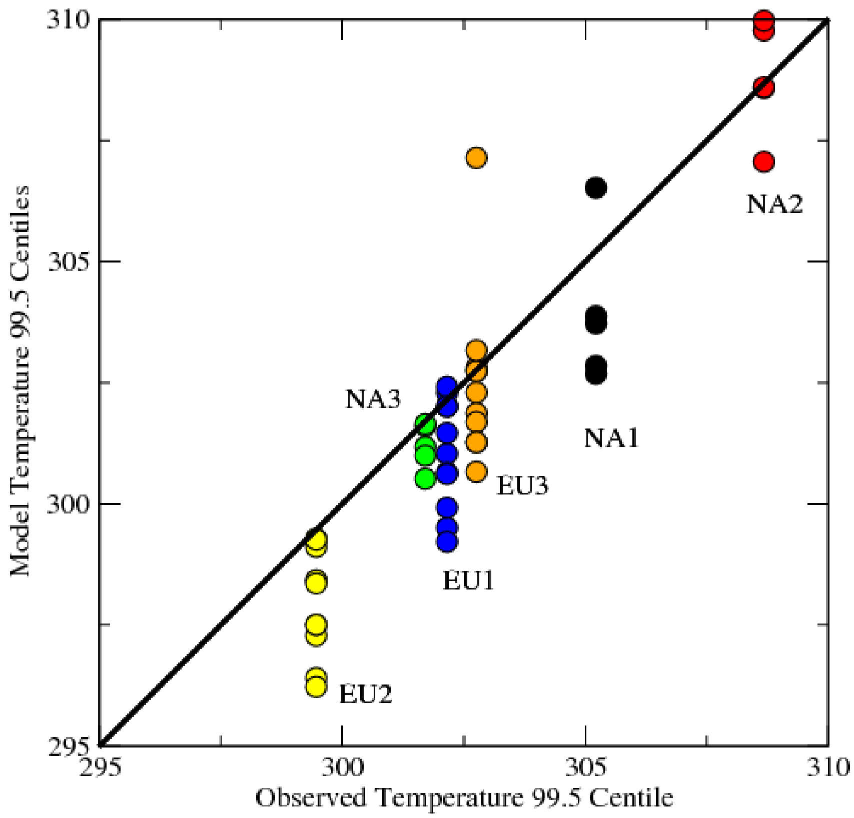

310
305
300
295
Model Temperature 99.5 Centiles
295
300
305
310
Observed Temperature 99.5 Centile
NA2
NA1
NA3
EU3
EU1
EU2

Figure 13

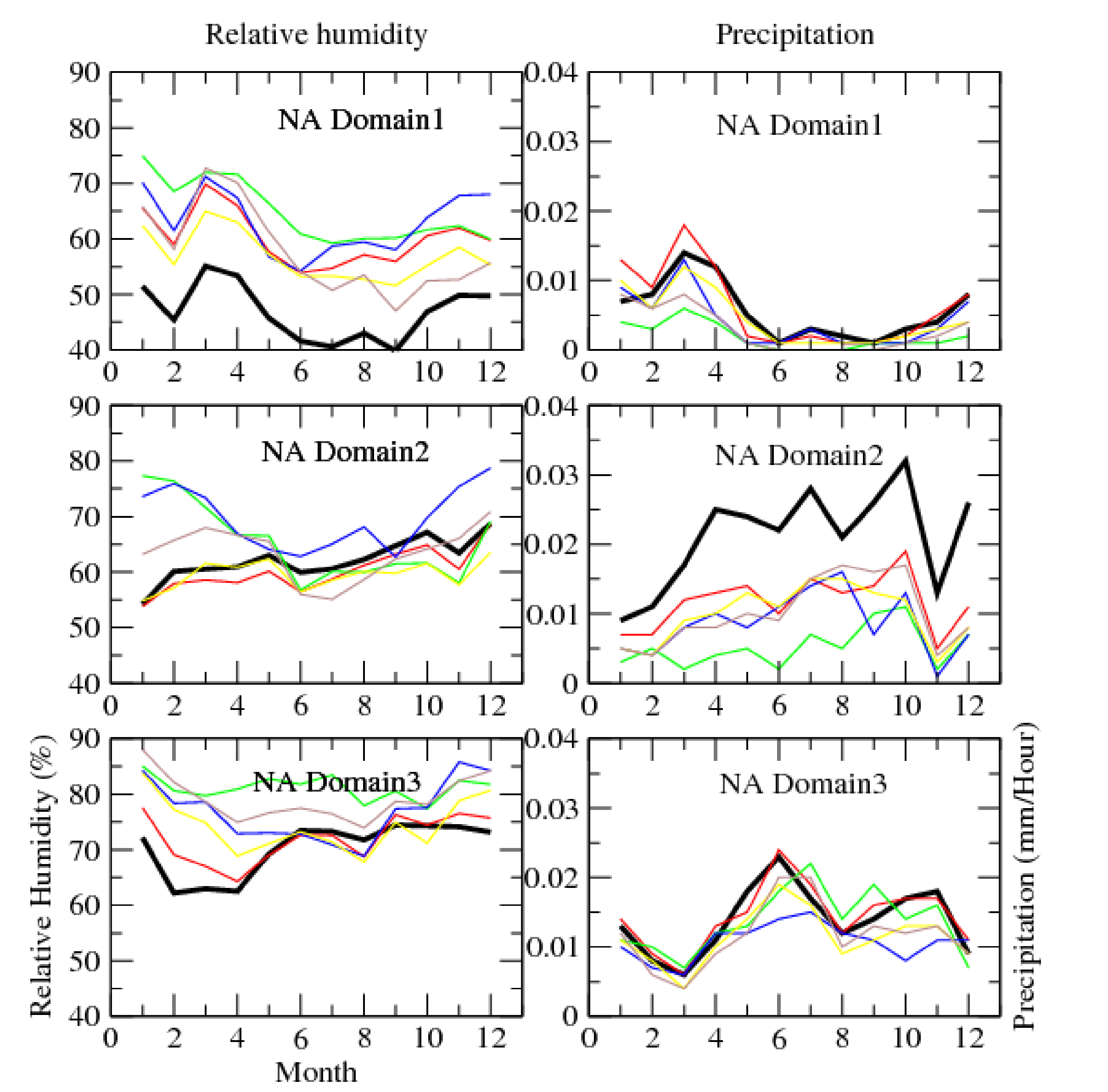

Relative humidity
Precipitation
NA Domain1
NA Domain2
NA Domain3
Relative Humidity (%)
Precipitation (mm/Hour)
Month

Figure 14

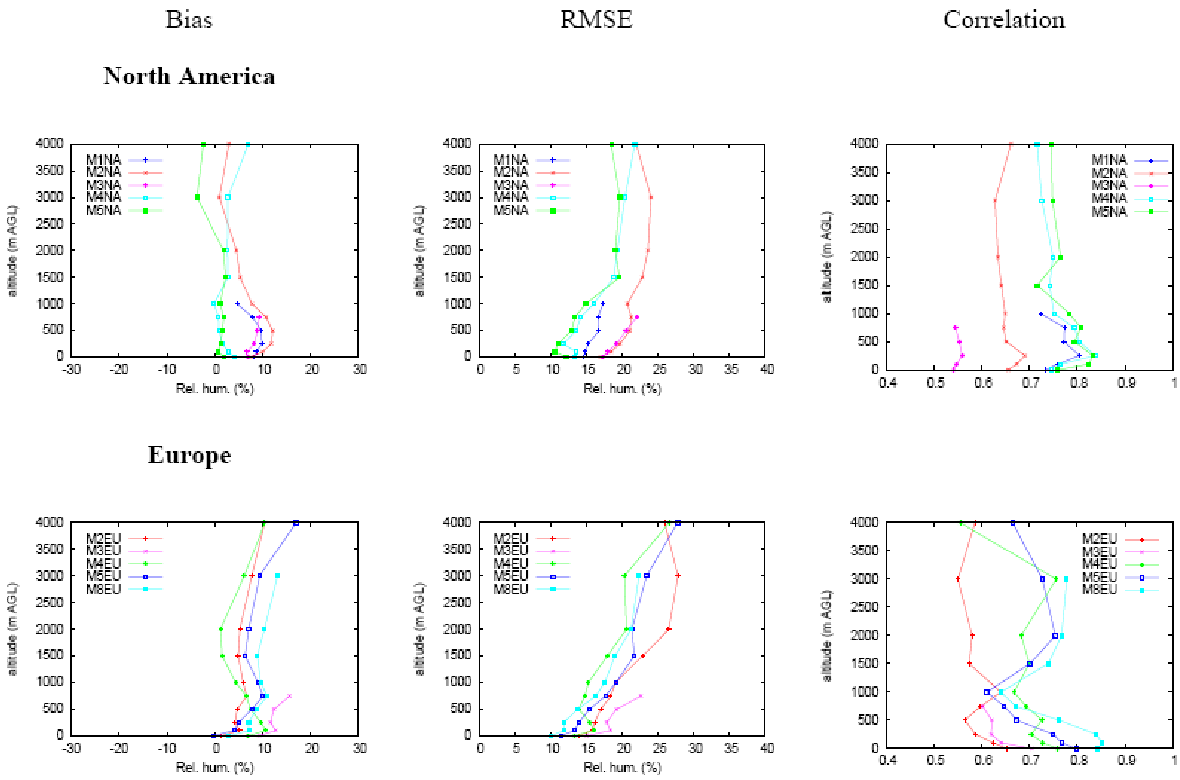
Bias
RMSE
Correlation
North America
M1NA
M2NA
M3NA
M4NA
M5NA
altitude (m AGL)
Rel. hum. (%)
Europe
M2EU
M3EU
M4EU
M5EU
M8EU

Figure 15

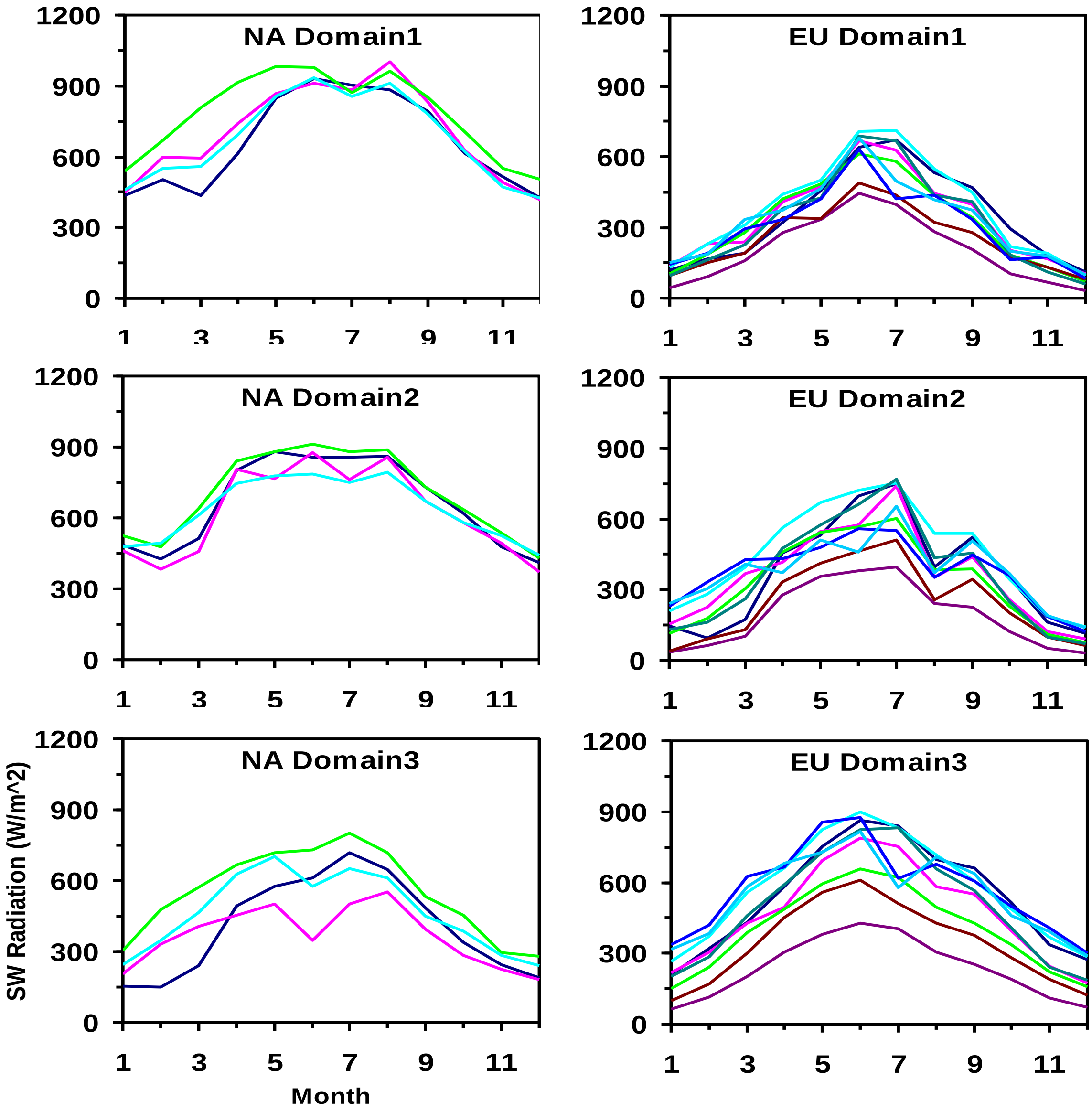

NA Domain1
EU Domain1
NA Domain2
EU Domain2
NA Domain3
EU Domain3
SW Radiation (W/m^2)
Month
1200
900
600
300
0
1
3
5
7
9
11

Figure 16

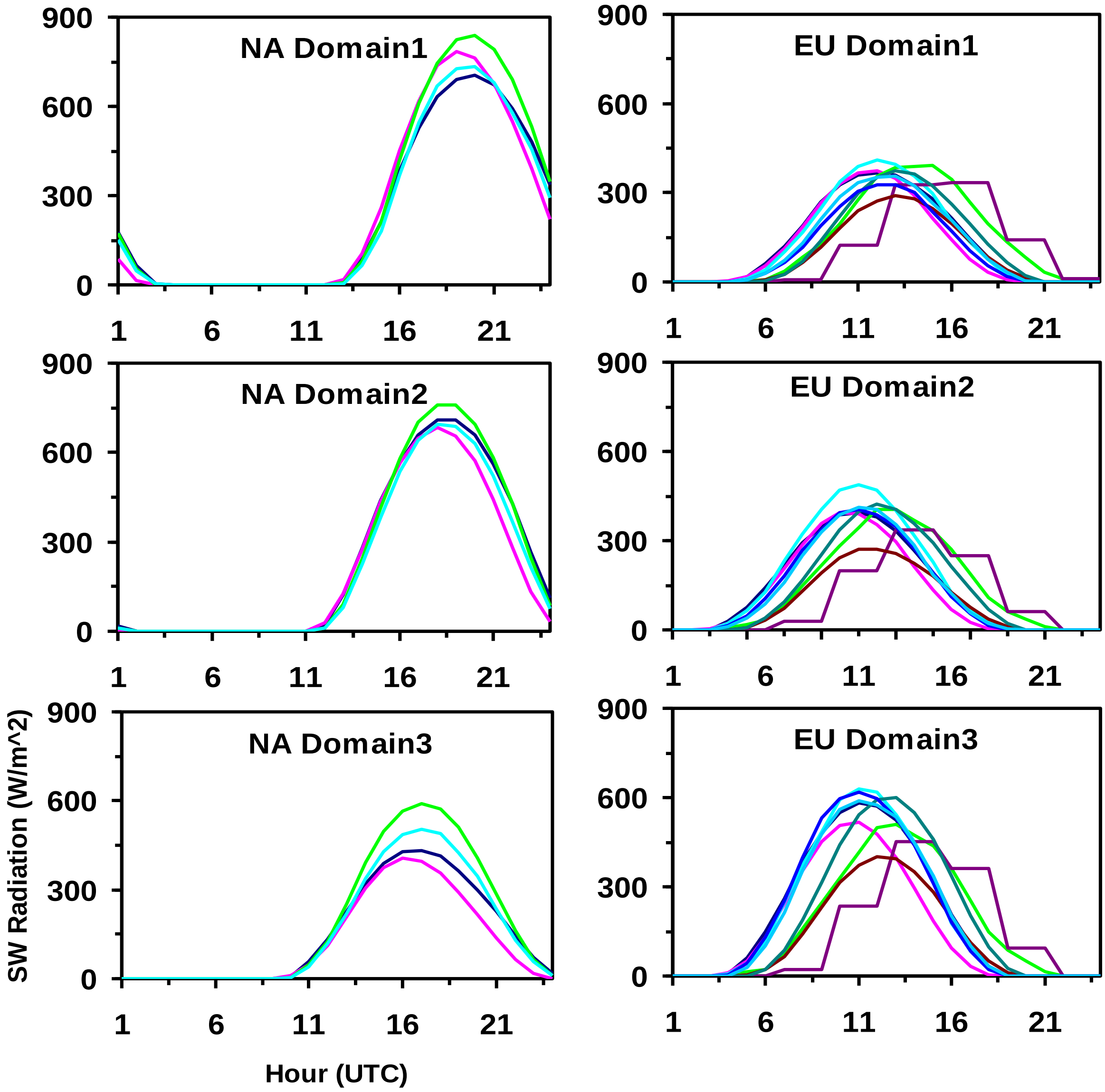
NA Domain1
EU Domain1
NA Domain2
EU Domain2
NA Domain3
EU Domain3
SW Radiation (W/m^2)
Hour (UTC)
900
600
300
0
1
6
11
16
21

Figure 17

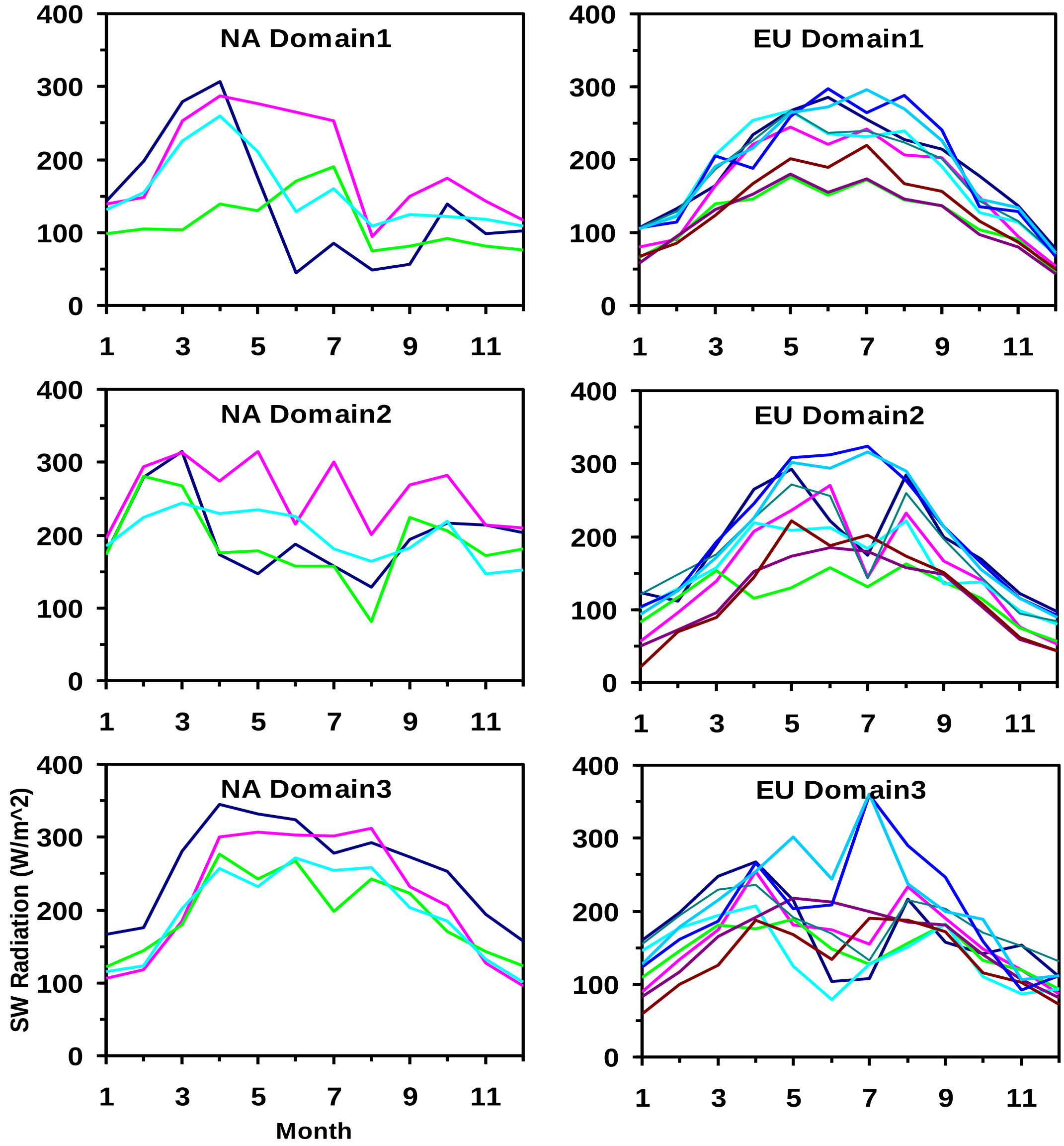

NA Domain1
EU Domain1
NA Domain2
EU Domain2
NA Domain3
EU Domain3
SW Radiation (W/m^2)
Month
400
300
200
100
0
1
3
5
7
9
11

Figure 18

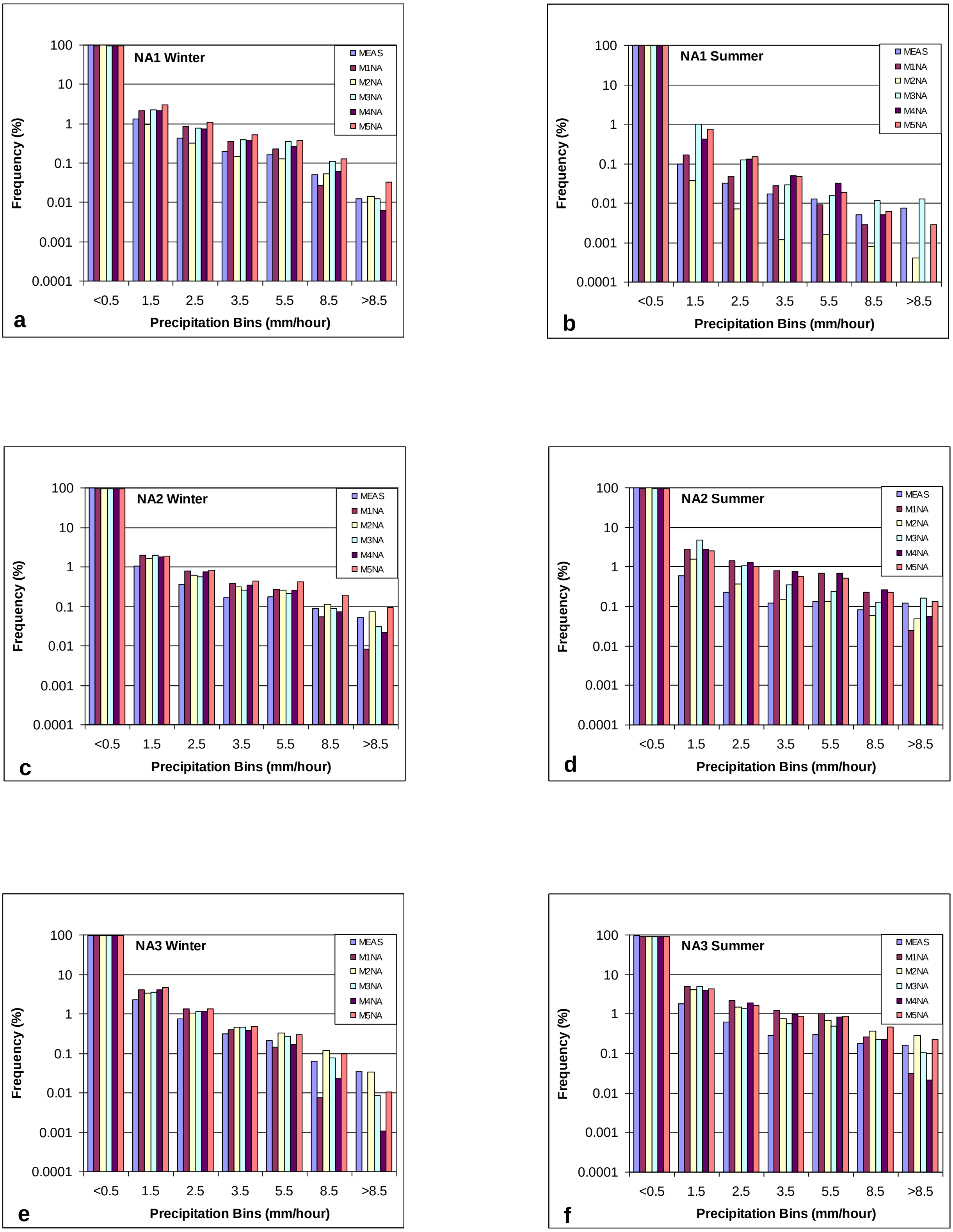
a
NA1 Winter
b
NA1 Summer
c
NA2 Winter
d
NA2 Summer
e
NA3 Winter
f
NA3 Summer
Frequency (%)
100
10
1
0.1
0.01
0.001
0.0001
Precipitation Bins (mm/hour)
<0.5
1.5
2.5
3.5
5.5
8.5
>8.5
MEAS
M1NA
M2NA
M3NA
M4NA
M5NA

Figure 19

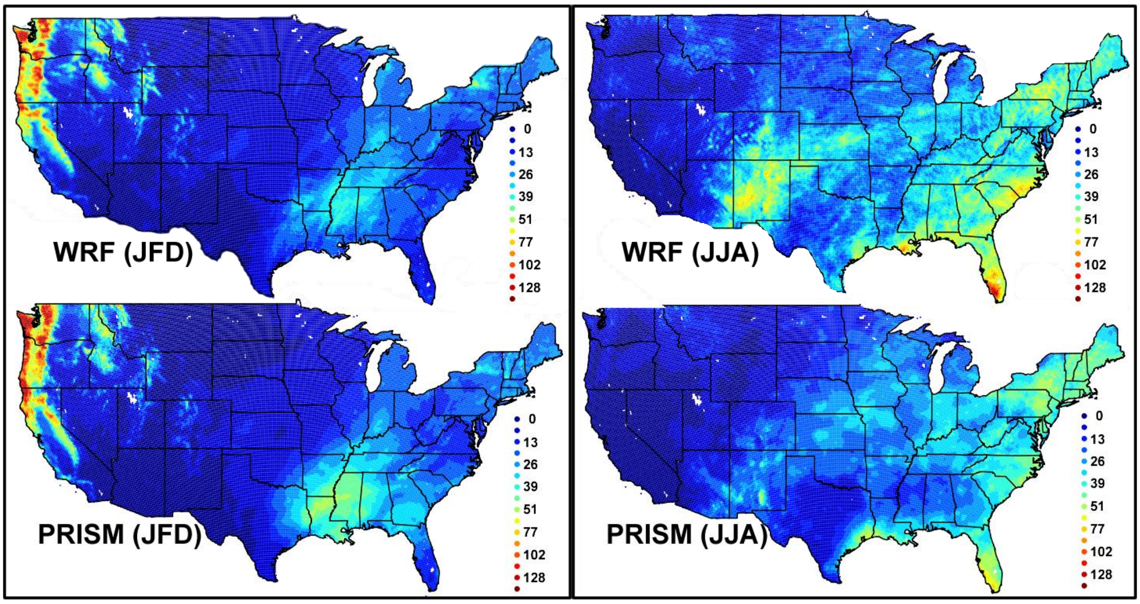

Figure 20